Blast-furnace slag cement and metakaolin based geopolymer as construction materials for liquid anaerobic digestion structures: Interactions and biodeterioration mechanisms

Marie Giroudon, Matthieu Peyre Lavigne, Cédric Patapy, Alexandra Bertron

Blast-furnace slag cement and metakaolin based geopolymer as construction materials for liquid anaerobic digestion structures: interactions and biodeterioration mechanisms

Marie Giroudon[1, 2] *, Matthieu Peyre Lavigne [2], Cédric Patapy [1], and Alexandra Bertron[1]

[1] LMDC, Université de Toulouse, UPS, INSA Toulouse, France

[2] TBI, Université de Toulouse, CNRS, INRA, INSA, Toulouse, France

*Corresponding author

Keywords: Anaerobic digestion, slag cement, geopolymer, biodeterioration, ammonium

Abstract

In order to promote the development of the biogas industry, solutions are needed to improve concrete structures durability in this environment. This multiphysics study aims to analyse the multiphases interactions between the liquid phase of an anaerobic digestion system and cementitious matrices, focusing on (i) the impacts of the binder nature on the anaerobic digestion process at local scale, and (ii) the deterioration mechanisms of the materials. Cementitious pastes made of slag cement (CEM III), innovative metakaolin-based alkali-activated material (MKAA), with compositions presumed to resist chemically aggressive media, and a reference binder, ordinary Portland cement (CEM I), were tested by immersion in inoculated cattle manure in bioreactors for a long period of five digestion cycles. For the first time it was shown that the digestion process was disturbed in the short term by the presence of the materials that increased the pH of the liquid phase and slowed the acids consumption, with much more impact of the MKAA. However, the final total production of biogas was similar in all bioreactors. Material analyses showed that, in this moderately aggressive medium, the biodeterioration of the CEM I and CEM III pastes mainly led to cement matrix leaching (decalcification) and carbonation. MKAA showed a good behaviour with very low degraded depths. In addition, the material was found to have interesting ammonium adsorption properties in the chemical conditions (notably the pH range) of anaerobic digestion.

1 Introduction

Biogas production is based on the degradation of organic matter by microorganisms under controlled anaerobic conditions (Chen et al., 2020; Huang et al., 2016; Yun et al., 2018). The process called anaerobic digestion consists of four consecutive degradation reactions: hydrolysis, acidogenesis, acetogenesis and methanogenesis (Batstone et al., 2002; Evans and Furlong, 2003; Wang et al., 2018) and has been evaluated as being one of the most energy-efficient and environmentally friendly technologies for bioenergy production (Fehrenbach et al., 2008; Yun et al., 2019, 2018). In the context of climate change and depletion of fossil resources, the development of anaerobic digestion structures is encouraged by the European Union, in particular through the European Directives 2001/77/EC and 2009/28/EC (2001, 2009). The process leads to the production of (i) a renewable energy source, biogas, which is mainly composed of methane (CH_4) and carbon dioxide (CO_2) (Lastella et al., 2002; Lesteur et al., 2010; Weiland, 2010) and (ii) a digestate that can be used as a fertilizer, due to nitrogen, phosphorous and potassium content and as the bioavailability of nitrogen is greater in the digestate than in the initial organic waste (Huang et al., 2016; Weiland, 2010). Optimized productivity is achieved in mesophilic conditions (usually 35°C) (Kothari et al., 2014) and at pH between 6.5 and 7.5 (Braun, 2007; Chandra et al., 2012; Liu et al., 2008). Although the anaerobic digestion technology is widely used, biogas production and digestate reutilization still need to be improved, in order to achieve maximum energy output. To this end, new strategies are being developed such as the co-digestion or the addition of accelerants, leading to a better degradation efficiency (Huang et al., 2016; Wang et al., 2019; Xu et al., 2020; Zhang et al., 2018). Anaerobic digestion plants can be set up with different types of organic waste and the biogas recovered can be used in many ways: production of heat, electricity, and vehicle fuel, or can even be injected after purification, into the network of natural gas (Frigon and Guiot, 2010; Holm-Nielsen et al., 2009; Yun et al., 2018).

The implementation of anaerobic digestion on an industrial scale requires airtight, isolated production structures. In this context, reinforced concrete, which is also an economical building material, is the most widely used material for the construction of digesters. Inside the digester, the cover concrete is in direct contact with the anaerobic digestion medium in the liquid phase, while polymeric liners or plastic layers are often applied to protect concrete in the gas phase (Nathalie Bachmann, 2013). At every stage of the digestion, the liquid medium contains species that are particularly aggressive to concrete (Koenig and Dehn, 2016; Voegel, 2017; Voegel et al., 2016, 2015), such as volatile fatty acids (VFA) (several g/L), ammonium (about 1 g/L) and dissolved CO_2 (several g/L). These species are responsible for concrete leaching (for VFA and ammonium) and/or carbonation (for dissolved CO_2) of the matrix (Bertron et al., 2005a; Magniont et al., 2011; Voegel et al., 2016). Moreover, the microorganisms colonize the concrete surface as a biofilm (Voegel et al., 2019a). Biofilms allow enhance the metabolic capacity of cells (Flemming et al., 2016) and seem to amplify the material deterioration, in terms of kinetics and intensity of alteration (Magniont et al., 2011). So far, few studies have investigated the fate of concrete exposed to fermenting biowaste. Koenig and Dehn (2016) studied the effects of anaerobic digestion in the liquid and gas phases of an industrial scale pilot digester. After 1 ½ years in the liquid phase, the authors observed erosion of the cover concrete and a degraded depth of 12.8 mm, with significant decalcification in the outer layer, features that are typical of an attack by acids, and precipitation of calcium carbonates. Voegel et al. (2019a, 2019b, 2016) identified deterioration mechanisms corresponding to a combination of decalcification and carbonation on cement paste specimens immersed in a synthetic biowaste for 4 weeks. The presence of alkaline cementitious materials slightly increased the pH (Voegel et al., 2015). Nevertheless, the liquid composition varies greatly over time and according to the substrate (Fisgativa et al., 2016; Li et al., 2015; Xu et al., 2019). Thus, depending on the type of biowaste, the composition in terms of VFA, ammonium and CO_2 varies and may impact the material differently. Moreover, these studies considered only classic cement matrices (based on CEM I, CEM II, CEM III or calcium aluminate cement). Thus, the degradation mechanisms of materials in anaerobic digestion

systems remain unknown for various liquid compositions and on innovative matrices. Furthermore, the impact of the materials on the process efficiency (biogas production) has never been studied.

The purpose of this laboratory study was to thoroughly evaluate the bio-geochemical interaction mechanisms between the anaerobic digestion medium and the materials at the local scale and their impact (i) on the quantitative and temporal production of methane and (ii) on the mineralogical and chemical alteration of the material that may compromise its long-term durability and thus the sustainability of the structure. In order to address these interface issues, the exploration strategy was to study the impact of different materials on anaerobic digestion by monitoring the liquid environment and the biogas production on the one hand, and to evaluate changes in the solid samples exposed to the medium on the other hand. Cement paste specimens made of blast-furnace slag cement (CEM III), a metakaolin-based alkali-activated geopolymer, and an ordinary Portland cement (OPC) paste (reference cement CEM I) were exposed to the liquid phase of inoculated cattle manure for more than 36 weeks. Ground Granulated Blast furnace Slag (GGBS) is a by-product of the iron industry and metakaolin is a powder obtained by calcination (600 to 800°C) and grinding of a clay mainly composed of kaolinite (AFNOR, 2012a). They may be used alone or as supplementary cementitious materials (SCM) with ordinary Portland cement (EN 206/CN, NF EN 197-1) (AFNOR, 2014, 2012b) to reduce the environmental impact of the cementitious material manufacturing by reducing the content of OPC, which is CO_2 emitter and energy-consuming (Juenger et al., 2019). Moreover, CEM III cement pastes had already shown increased durability to acid attacks compared to ordinary Portland cement (CEM I) due to the addition of aluminium-rich ground granulated blast-furnace slag (Bertron et al., 2005b; Gruyaert et al., 2012; Oueslati and Duchesne, 2012). The slag addition increases the chemical resistance to material leaching by decreasing the calcium content of the binder and leads to a reduced portlandite content, a lower Ca/Si ratio of C-S-H[1] – the main hydrated phase of the material – and the formation of C-A-S-H (Elakneswaran et al., 2016;

[1] Cement chemistry shorthand notations: A = Al_2O_3, C = CaO, F = Fe_2O_3, H = H_2O, M = MgO, S = SiO_2

Lothenbach et al., 2011), with higher chemical stability than C-S-H (Roosz et al., 2018). Furthermore, the addition of slag to cement helps to densify the paste by filling the large pores with hydration products and the resulting finer pore structure improves the transfer properties of the paste (Perlot et al., 2006). The French prescription guide T47 (CIMbéton, 2009) recommends slag cements for use in aggressive chemical media and they are actually used in the design of concrete for digester structures. On the other hand, geopolymers have shown encouraging behaviour when exposed to acidic abiotic (Drugă et al., 2018; Duan et al., 2015; Singh et al., 2015) and biotic (Grengg et al., 2020; Khan et al., 2017) environments. However, the chemical and mineralogical compositions of geopolymers are very variable and some of them, such as fly ash geopolymers (Khan et al., 2018), and pure white metakaolin geopolymer (Grengg et al., 2020), showed poor resistance to microbially induced deterioration (MID). The behaviour of these matrices therefore needs to be studied in order to assess their suitability for use in an anaerobic digestion environment.

Cement paste specimens were exposed to the fermenting biowaste in biochemical methane potential reactors with a high solid/liquid ratio in order to reproduce local chemical conditions in the vicinity of the concrete walls of the digester. The liquid and gas phases were monitored over time. Scanning Electronic Microscopy (SEM) observations coupled with Electron Probe Micro-Analysis (EPMA), and X-Ray Diffraction (XRD) analyses were used to investigate the chemical and mineralogical changes of the specimen.

2 Materials and methods

The experimental protocol implemented in this study is presented in Figure 1. It consisted of a series of bioreactors where construction materials samples were immersed in inoculated cattle manure at mesophilic temperature (35°C) in order to reproduce anaerobic digestion conditions. During the 256 days experiment (5 cycles of anaerobic digestion), both gas and liquid phases were monitored (see section 2.3) while the chemical and mineralogical changes occurred in the cementitious material samples were analysed at the end of the third and fifth cycles (see section 2.5).

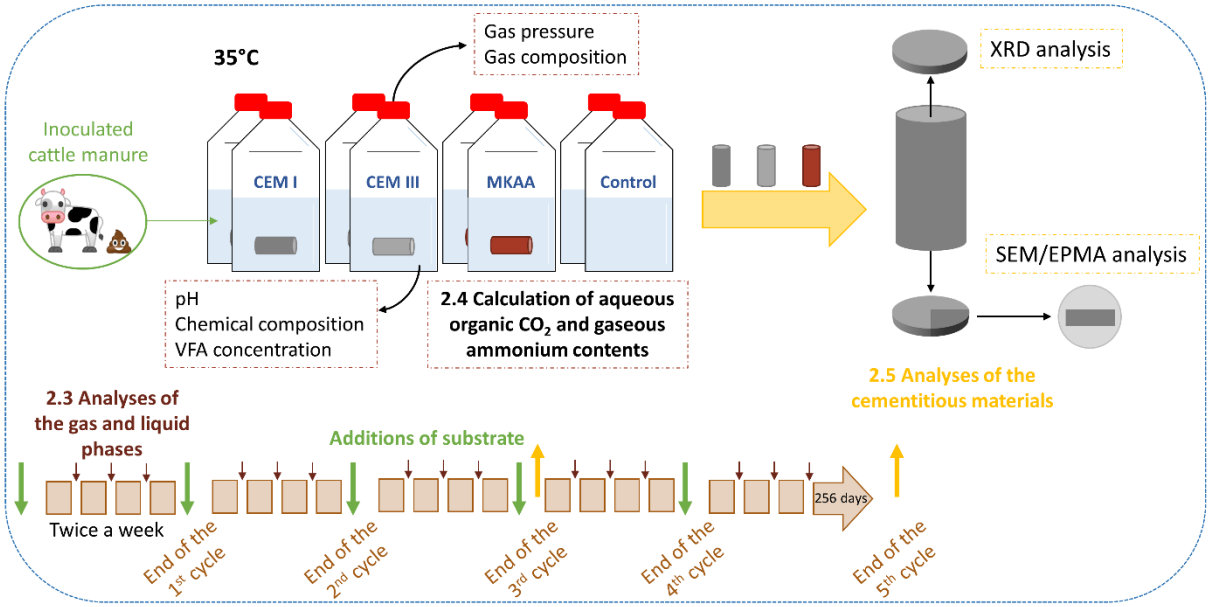

Figure 1: Schematic representation of the experimental protocol to study the interactions between the anaerobic digestion environment and the cementitious materials

2.1 Binder materials

Cement pastes made of CEM III/B 42.5N (CEM III), a mixture of Portland cement and GGBS, and an ordinary Portland cement CEM I 52.5R (CEM I), were poured with a water/binder ratio of 0.30. The metakaolin-based alkali-activated (MKAA) paste was made with the following molar ratio – $\frac{SiO_2}{Al_2O_3} = 3.6$; $\frac{Na_2O}{Al_2O_3} = 0.9$; $\frac{H_2O}{Na_2O} = 14.5$ – by using metakaolin (Argeco), liquid sodium silicate (molar ratio $\frac{SiO_2}{Na_2O} = 1.7$) and water. The metakaolin used in this study came from the calcination of a kaolin with a relatively high level of impurity and included quartz (45%), mullite (2%), calcite (1%), anatase (1%) and kaolinite (1%), as well as a considerable amount of iron oxide (3.7% of Fe_2O_3) (Pouhet, 2015; San Nicolas et al., 2013).

A procedure adapted from the French standard NF EN 196-1 (AFNOR, 2016) was used to mix the paste specimens, i.e., for each cement paste, the binder and the water were mixed at low speed (140 ± 5 rpm) for 60 seconds and at high speed (285 ± 10 rpm) for 90 seconds. The pastes were cast in cylindrical moulds 75 mm high and 25 mm in diameter. Each specimen was protected from the atmosphere by a plastic coating after pouring. 24h after pouring, the CEM III and CEM I pastes were removed from their moulds, sealed in plastic bags and kept at 20°C for a 27-day endothermic cure. MKAA pastes were cured for 7 days in their closed moulds and then stored in sealed plastic bags. At 28 days of maturation, the paste specimens were exposed to the fermenting biowaste.

2.2 Preparation of laboratory reactors and immersion of cement pastes

To start, 100 mL of microbial inoculum collected from an industrial biogas plant in Haute-Garonne (France) and cattle manure from the experimental farm of the Engineering School of Purpan (France) (the substrate) were poured into airtight biochemical methane potential (BMP) reactors (Holliger et al., 2016). For each kind of material, the experiment was carried out in duplicate with two bioreactors each containing a sample. In addition, two control bioreactors without material were also taken into account.

Immediately after the first feed with substrate, the paste specimens were immersed in bioreactors. The solid/liquid ratio (cement paste surface area/total liquid volume) was approximately 85 $cm^2.L^{-1}$, much higher than the in situ ratio in a standard industrial digester of approximately 4 $cm^2.L^{-1}$ (Voegel et al., 2015). This ratio was chosen high in order to reproduce and emphasize local phenomena in the vicinity of the concrete wall, where the chemical conditions are strongly influenced by the interactions between the biowaste and the cement matrix.

After the immersion of the samples, water was added to reach a volume of 800 mL and the gas phase was flushed with N_2 in order to remove O_2. The bioreactors were maintained at 35°C in an oven for 5 cycles. At each new cycle, the liquid medium from the previous cycle was kept in the reactors, supplemented with water (to reach the initial volume of 800 mL) and small amounts of new cattle

manure were incorporated (Table 1). The mass of cattle manure added increased with the cycles in order to offset a decrease in the substrate's methanogenic potential over time. Each cycle was considered complete when the gas production in the control reactors stopped, except for the last cycle which lasted until the biogas production was over in all the bioreactors (see durations in Table 1). During the fourth cycle, once the biogas production was complete, the reactors were kept at ambient temperature for 6 weeks because the laboratory closed for the summer break.

Table 1: Approximate mass of cattle manure added per cycle and duration of each cycle

	1st cycle	**2nd cycle**	**3rd cycle**	**4th cycle**		**5th cycle**
Temperature	35°C	35°C	35°C	35°C	Room	35°C
Mass of cattle manure added (g)	6	6	8	10		13
Duration of cycle (weeks)	7	6.5	5	4	6	8

2.3 Sampling and analysis of the anaerobic digestion medium

Twice a week, the gas pressure was measured and liquid was sampled. If the gas pressure was above 0.250 bar, some gas was sampled for analysis (O_2/N_2, H_2, CH_4 and CO_2) by gas chromatography (GC Trace 1300 Thermofisher) and the gas pressure was then brought back to ambient pressure. Samples of 5 mL of the liquid medium were collected and the pH of each sample was measured. The liquid samples were centrifuged (Eppendorf, Centrifuge 5430R) for 5 minutes (4°C, RCF 7197). In one hand, the concentrations of ionic species PO_4^{3-}, Na^+, NH_4^+, K^+, Cl^-, Ca^{2+} and Mg^{2+} were analysed by Ion Chromatography (Dionex Thermofisher DX320). In the other hand, 1 mL of the supernatant part was sampled and mixed with 0.5 mL of an internal standard (solution of 2-ethyl-2-butyric acid at 1 $g.L^{-1}$ in demineralized water and containing 5% orthophosphoric acid H_3PO_4) to be analysed by gas chromatography (Varian SERIE 3900/430) in order to provide the concentrations of some VFA (acetic, propionic, isobutyric, butyric, isovaleric, and valeric acids).

2.4 Calculation method for aqueous inorganic CO_2 and gaseous ammonium contents

As the analyses carried out did not allow the aqueous inorganic CO_2 and gaseous ammonium contents to be measured, gas and liquid chromatography results, together with thermochemical equilibria associated with Henry's law, were used to calculate these missing data.

2.4.1 Theoretical background: Henry's Law

Henry's law states that the partial pressure of the dilute solute in a solution is directly proportional to its liquid mole fraction. The proportionality factor is called the "Henry's law constant" (H_i) (Equation A).

$$Py_i = H_i x_i \quad \text{(A)}$$

In Equation A, P, y_i, H_i and x_i are the total pressure, the composition of solute in vapour gas (molar fraction of the gas phase), Henry's law constant of solute i , and the molar fraction of the liquid phase, respectively.

The constants were calculated considering a temperature of 35°C, the atmospheric pressure and the pH after each gas sampling (values of the Henry's law constants from Batstone et al. (2002)).

2.4.2 Aqueous inorganic CO_2 content

The inorganic CO_2 content corresponds to the molar fraction of the liquid phase x_{CO_2} divided by the water concentration, 55.41 mol.L^{-1} (Equation B).

$$\left[CO_{2\,aq}\right] = \frac{x_{CO_2}}{55.41} \text{ where } x_{CO_2} = \frac{P_{atm} y_{CO_2}}{H_{CO_2}} \quad \text{(B)}$$

Using the thermochemical equilibria (Reactions 1 and 2), and the gas composition, the total inorganic CO_2 content can be calculated by successively calculating the $[HCO_3^-]$ and $[CO_3^-]$ concentrations.

$$H_2CO_3 + H_2O \rightleftharpoons HCO_3^- + H_3O^+, K_{C_1} \quad \text{(1)}$$

$$HCO_3^- + H_2O \rightleftharpoons CO_3^- + H_3O^+, K_{C_2} \quad (2)$$

where K_{C_1} and K_{C_2} are the thermodynamic equilibrium constants, values from Batstone et al. (2002). K_{C_1} = 4.73E^{-7} and K_{C_2} = 5.60E^{-11} at 35°C.

2.4.3 Gaseous ammonium content

Using the thermochemical equilibria (Reaction 3) and the total ammonium concentration in the liquid phase, the $[NH_4^+]$ and $[NH_3]_{aq}$ concentrations were calculated.

$$NH_4^+ + H_2O \rightleftharpoons NH_3 + H_3O^+, K_N \quad (3)$$

where K_N is the thermodynamic equilibrium constant, value from Batstone et al. (2002). K_N = 6.16E^{-10} at 35°C.

Henry's law then allowed the gaseous ammonium content to be calculated, assuming equilibrium and no limitation of liquid/gas transfer (Equation C):

$$y_{NH_3} = \frac{x_{NH_3} H_{NH_3}}{P_{atm}} \text{ where } x_{NH_3} = \frac{[NH_3]_{aq}}{55.41} \quad (C)$$

2.5 Analysis of cementitious materials

At the end of each cycle, the cylindrical cement paste specimens were removed from the bioreactors and a diamond saw was used to collect slices for solid analyses. Quarter sections were intended for SEM and EPMA analysis. They were embedded in an epoxy resin (Mecaprex Ma2+ from Presi), and dry polished using silicon carbide polishing disks (Presi) (Bertron et al., 2009). Then, the polished sections were coated with carbon. Analyses by SEM (JEOL JSM-LV, 15 kV) combined with EPMA analyses (Cameca SXFive, 15 kV, 20 nA) enabled the microstructural and chemical characterization of the specimens. For EPMA, the points to be analysed were chosen to avoid residual anhydrous grains. Chemical profiles were established from the surface in contact with the liquid phase to the core of the specimen. For each point, the following elements were analysed: Ca, Si, Al, Fe, Mg, S and P. Element mass percentages were expressed as mass percentages of the associated oxides.

The mineralogical composition changes of the specimens were characterized by XRD (Brucker D8 Advance, Co cathode, 40 kV, 40 nA). The plane side of the slice, which was directly in contact with the liquid medium, was first analysed. Then, the sample was abraded in order to characterize the degradation in depth, and this until reaching the sound material (Bertron et al., 2005a).

XRD and EPMA analyses were performed after the third cycle. SEM observations were carried out after each cycle.

3 Results

3.1 Characteristics of the liquid phase according to the material during the anaerobic digestion

3.1.1 Biogas production and composition

Figure 2 gives the total production of CH_4 per gram of cattle manure in each type of bioreactor and the cumulative total production at the end of the experiment. Mean values of the two duplicate bioreactors are presented with the standard deviations.

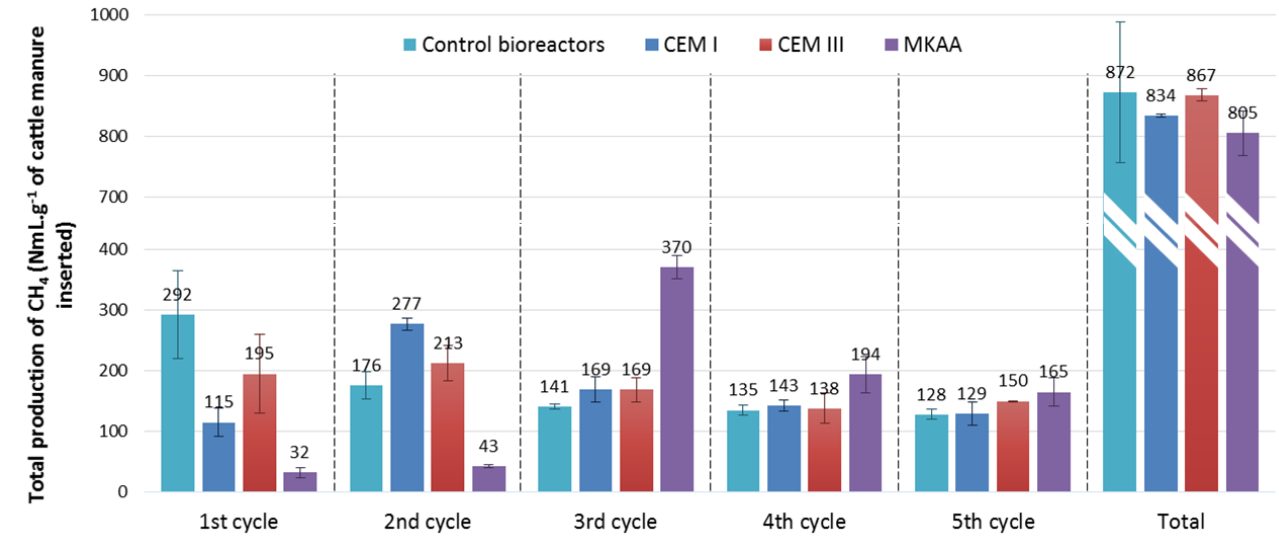

Figure 2: Total production of CH_4 (NmL.g^{-1} of cattle manure) at the end of each digestion cycle and cumulative total production at the end of the experiment (Total)

In the control bioreactors, the production of CH_4 reached between 292 and 128 NmL of CH_4 per gram of cattle manure per cycle. The decrease of the methane production as the number of cycles increased expresses a decrease in the methanogenic potential of the substrate over time, which was probably due to the evolution of the cattle manure during the storage (4°C) time of the experiment.

The presence of the cementitious materials CEM I and CEM III, induced a significantly lower methane production during the first cycle than that in the control bioreactors (292 NmL of CH_4/g of cattle manure) with 115 and 195 NmL, respectively, of CH_4 per gram of cattle manure. During the second cycle, the bioreactors containing the CEM I and CEM III samples showed methane production rates (respectively 277 and 213 NmL of CH_4/g of cattle manure) that were higher than those of the control bioreactors (176 NmL of CH_4/g of cattle manure). Thereafter, production in the bioreactors containing cementitious materials was equivalent to those of the control bioreactors.

The biogas production in the bioreactors containing alkaline MKAA was strongly delayed compared to other bioreactors. About ten times less methane (32 NmL of CH_4 per gram of cattle manure) was produced in the MKAA bioreactors than in the control bioreactors during the first cycle and the production remained very low (43 NmL of CH_4 per gram of cattle manure) during the second cycle. The third cycle was marked by a sharp increase of methane production in these bioreactors (370 NmL of CH_4 per gram of cattle manure). During the fourth and fifth cycles, methane production in the MKAA reactors remained slightly higher than in the control bioreactors.

Even if the presence of the materials delayed the biogas production, at the end of the experiment the cumulative amount of methane produced was equivalent for all the bioreactors (-4.4%, -0.6% and -7.7% relative to the control for CEM I, CEM III and MKAA, respectively).

Table 2 gives the composition of the gas phase (N_2, CH_4, CO_2) of the bioreactors at the end of each cycle in volume percent. Mean values of the two duplicate bioreactors are presented with the standard deviations.

Table 2: Composition of the gas phase (N_2, CH_4, CO_2) at the end of each cycle (vol.%)

	%	End of 1st cycle	End of 2nd cycle	End of 3rd cycle	End of 4th cycle	End of 5th cycle
Control	**N_2**	24.5 ± 3.2	32.5 ± 3.8	31.7 ± 1.1	33.9 ± 1.4	27.9 ± 1.8
	CH_4	54.5 ± 1.7	42.5 ± 1.5	42.8 ± 0.4	44.7 ± 0.4	46.8 ± 1.5
	CO_2	22.6 ± 1.6	23.0 ± 2.4	24.0 ± 0.8	19.4 ± 1.2	25.3 ± 0.1
CEM I	**N_2**	64.2 ± 7.1	33.7 ± 1.1	34.5 ± 5.0	31.4 ± 2.1	23.8 ± 2.6
	CH_4	34.8 ± 6.4	48.8 ± 1.2	43.9 ± 3.1	44.0 ± 2.7	48.4 ± 1.0
	CO_2	2.6 ± 0.8	15.1 ± 2.4	20.1 ± 1.3	21.2 ± 1.8	27.6 ± 2.0
CEM III	**N_2**	49.2 ± 13.3	34.2 ± 6.4	32.6 ± 4.8	35.8 ± 5.7	24.7 ± 1.6
	CH_4	45.3 ± 8.7	46.9 ± 5.8	45.4 ± 2.6	44.8 ± 3.4	49.6 ± 0.3
	CO_2	7.1 ± 4.5	17.3 ± 0.7	20.2 ± 1.9	17.6 ± 1.8	25.1 ± 1.7
MKAA	**N_2**	87.5 ± 2.9	81.4 ± 1.1	16.6 ± 1.2	26.7 ± 4.7	21.6 ± 4.5
	CH_4	12.3 ± 3.2	15.1 ± 0.9	62.7 ± 1.3	52.9 ± 1.2	49.9 ± 3.4
	CO_2	0.1 ± 0.0	0.6 ± 0.0	15.5 ± 2.7	17.2 ± 3.4	28.0 ± 0.4

Table 2 shows that the composition of the gas phase in the control bioreactors varied little over time, with about twice as much CH_4 as CO_2, and approached the composition of an industrial biogas (55 to 65% of CH_4 and 30 to 40% of CO_2 (Rasi, 2009)). In contrast, in the bioreactors containing the materials, the proportion of N_2 decreased through the cycles since more and more biogas was produced. Moreover, the proportion CO_2/CH_4 varied depending on materials and time. While it was almost constant in the control bioreactors (about 1/2), this ratio was very low in the bioreactors containing materials during the first cycle. It then increased (more slowly in the bioreactors containing MKAA due to the delay of the efficient biogas production) and tended to reach ½ thereafter.

3.1.2 *pH and volatile fatty acids production*

Figure 3 gives the evolution of the pH during the five cycles of anaerobic digestion in the liquid fraction of the bioreactors.

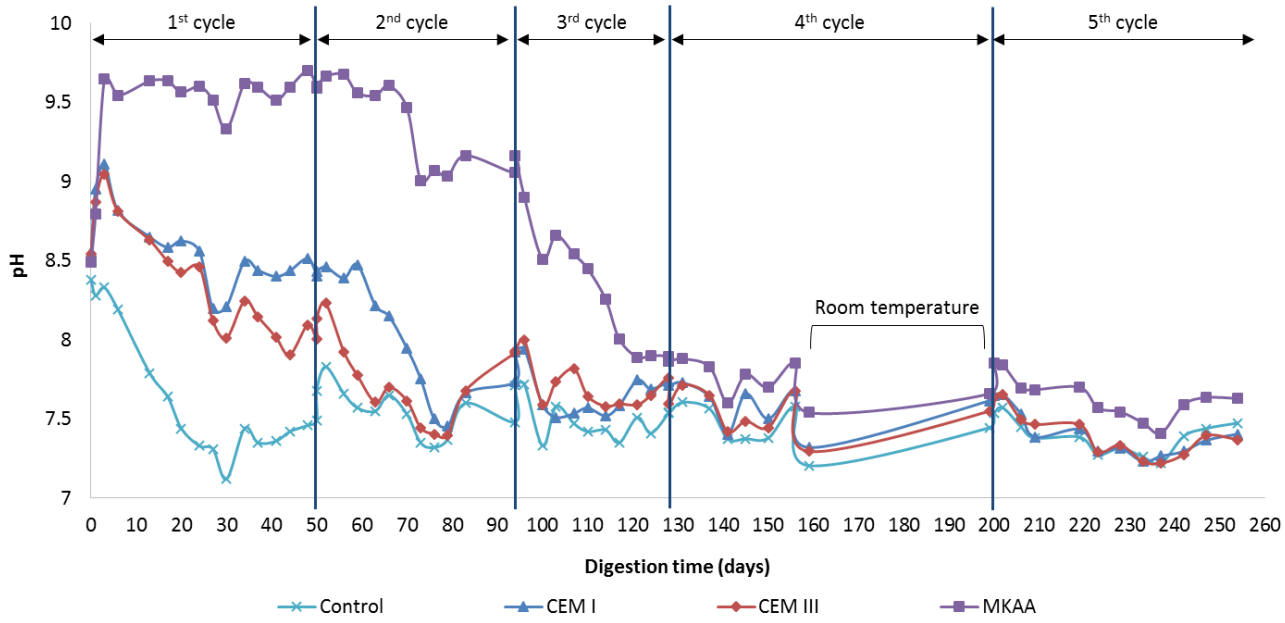

Figure 3: Evolution of the pH during the five cycles of anaerobic digestion in the bioreactors

At the start of the first digestion cycle (day 0) the pH was identical in all the bioreactors (pH = 8.5 ± 0.1). The subsequent measurements showed very different behaviours among the bioreactors. The control bioreactors first underwent a decrease of pH during the first 30 days. From the second cycle, the pH reached suitable values for anaerobic digestion and remained stable between 7.3 and 7.8 for the rest of the experiment.

The alkalinity of the cementitious materials (CEM I and CEM III) impacted the pH which increased significantly in the first few days, reaching a maximum of about 9 on day 3. Thereafter, the negative effect of the cementitious materials seems to have been overcome and the pH decreased, until values similar to those of the control bioreactors were observed at day 76. At the same time, biogas production accelerated in these bioreactors.

285 Singular behaviour was observed in the bioreactor containing the MKAA. As for the bioreactors
286 containing cementitious materials, the pH first increased due to the high alkalinity of the material.
287 However, it reached a very high value, of 9.6, on the third day. The pH remained at this high value
288 during the first cycle and started to decrease halfway through the second cycle, on day 70. During
289 the third cycle, a rapid decrease of pH was observed in the MKAA bioreactors, and pH conditions
290 approached those of production in the other bioreactors. This pH drop occurred at the same time as
291 biogas production started.

292 During the fourth and fifth cycles, the pH was stable for all types of bioreactors. However, it was
293 observed that the pH in the MKAA bioreactors remained about 0.3 higher than in the others.

294 Figure 4 gives the total acid concentrations in the liquid phase of the bioreactors during the
295 experiment. Among the VFA typically metabolized by microorganisms in anaerobic digestion (acetic,
296 propionic, butyric, isobutyric and isovaleric acids) (Cibis et al., 2016), acetic acid was predominant far
297 ahead of the others, as in several previous studies (Koenig and Dehn, 2016; Voegel et al., 2019b,
298 2016). The choice was thus made to present the total acid concentration for each material.

299 The first cycle showed a significant increase in the VFA concentration at the start of the digestion.
300 Thereafter, two different types of behaviour occurred.

301 For the control bioreactors and the bioreactors containing CEM I and CEM III, the production reached
302 a maximum during the second week, with concentrations of 0.35 $g.L^{-1}$, 0.26 $g.L^{-1}$ and 0.29 $g.L^{-1}$
303 respectively. This initial increase corresponded to the acidogenesis step and was followed by the
304 slow consumption of the VFA marking the continuation of the digestion of the cattle manure.
305 Although the CEM I, CEM III and control bioreactors shared similar behaviour, it was observed that
306 the materials had an impact (i) on the quantity of VFA produced, the CEM I bioreactors producing
307 0.09 $g.L^{-1}$ less acid than the control ones, and (ii) on the kinetics of production: the decrease in the
308 total acid concentration was slower in the bioreactors containing materials and some VFA remained
309 at the end of the first cycle, highlighting a less efficient consumption of VFA. This induced a new,

smaller increase in the VFA concentration at the start of the second cycle. Thereafter, the VFA were well consumed and their concentration increased only very little at the start of subsequent cycles.

During the first 17 days, the evolution of the VFA concentration in the MKAA bioreactors followed the same trend as in the other bioreactors. Afterwards, the VFA concentration in the MKAA bioreactors presented a different evolution: instead of decreasing, it continued to increase during the first cycle and the accumulation of VFA accelerated with the start of the second cycle. The VFA concentration reached 1.58 $g.L^{-1}$ on day 103 and suddenly dropped to only 0.09 $g.L^{-1}$ at the end of the third cycle (day 128). This behaviour was strongly linked to the pH since the drop in the VFA concentration occurred just after the pH decrease.

In the fourth and fifth cycles, all the bioreactors had low concentrations of VFA, showing their good consumption during the anaerobic digestion.

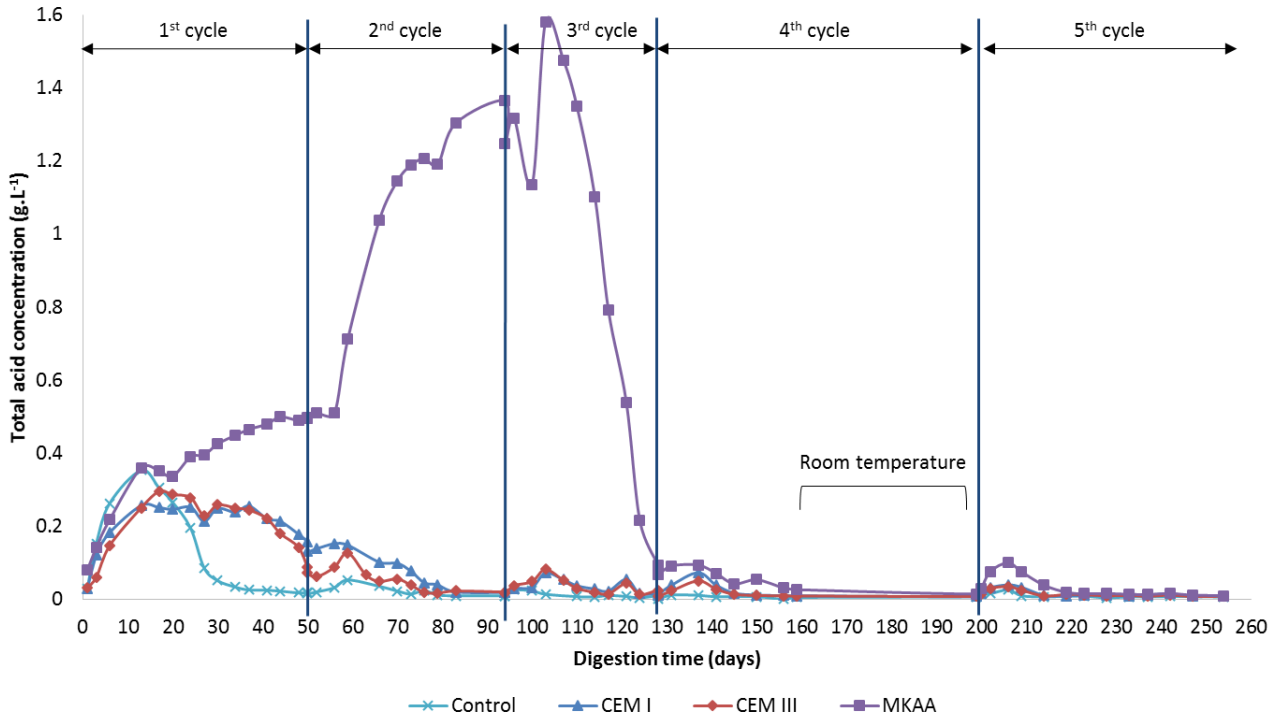

Figure 4: Evolution of the total acid concentration during the five cycles of anaerobic digestion in the bioreactors

3.1.3 *Ammonium concentration*

Figure 5 shows the evolution of the ammonium concentration during the anaerobic digestion of cattle manure in the bioreactors.

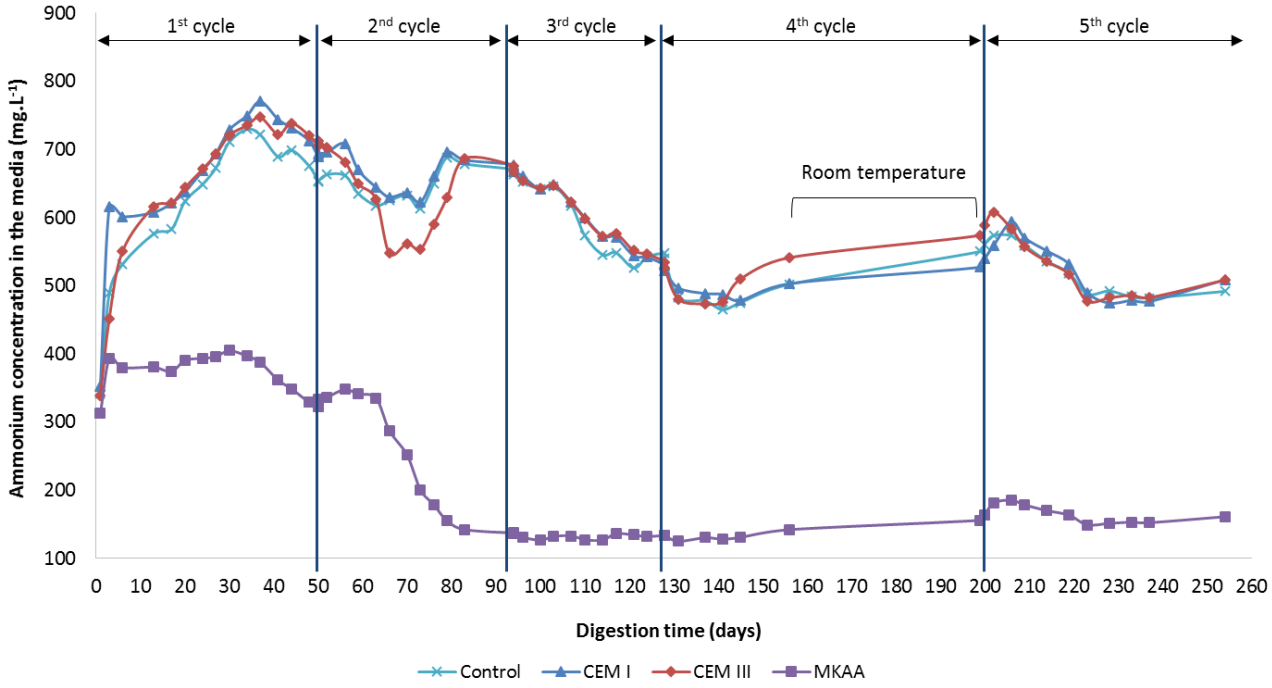

Figure 5: Evolution of the ammonium concentration during the anaerobic digestion of cattle manure in the bioreactors

In anaerobic digestion, ammonium is present in the substrate and is also produced by the degradation of some proteins (Yenigün and Demirel, 2013), depending on the biowaste or the inoculum. In our case, it can be observed that the initial addition of inoculum and substrate induced a significant increase of the ammonium concentration while the following additions of substrate did not lead to such an increase. Thus, ammonium was provided by the inoculum and not by the biowaste. Once again, the singular behaviour of the bioreactor containing the MKAA can be noted.

In the bioreactors containing the cementitious materials and in the control bioreactors, the ammonium content reached about 750 $mg.L^{-1}$ after 30 days of digestion. After this initial increase, the ammonium concentrations tended to fall slowly through cycles, probably due to the consumption of ammonium for the growth of the microbial communities (Kuypers et al., 2018).

The ammonium concentrations were much lower (about 400 $mg.L^{-1}$) in the bioreactors containing MKAA during the first cycle and dropped during the second cycle. The ammonium concentration remained around 130 $mg.L^{-1}$ for the rest of the experiment. This will be investigated further in the discussion section.

3.1.4 Release of ions in solution

Table 3 gives the Na^+, K^+, PO_4^{3-} and Mg^{2+} concentrations ($mg.L^{-1}$) in the liquid phase of the bioreactors at the start of each cycle. Mean values of the two duplicate bioreactors are presented with the standard deviations.

Table 3: Na^+, K^+, PO_4^{3-} and Mg^{2+} concentration ($mg.L^{-1}$) in the liquid phase of the bioreactors at the start of each cycle

	$mg.L^{-1}$	**Start of the 1st cycle**	**Start of the 2nd cycle**	**Start of the 3rd cycle**	**Start of the 4th cycle**	**Start of the 5th cycle**
$[Na^+]$	**Control**	117.5 ± 13.4	167.0 ± 1.7	125.6 ± 0.9	149.8 ± 120.8	121.3 ± 0.9
	CEM I	130.5 ± 13.4	195.5 ± 9.8	155.6 ± 2.2	154.4 ± 3.4	138.4 ± 2.7
	CEM III	123.5 ± 0.7	197.6 ± 0.4	145.9 ± 1.6	140.4 ± 1.9	142.6 ± 1.2
	MKAA	636.0 ± 77.4	2222.2 ± 80.6	1749.3 ± 61.2	1908.1 ± 2.2	2007.9 ± 13.1
$[K^+]$	**Control**	231.0 ± 19.8	379.1 ± 11.6	292.3 ± 9.9	390.7 ± 18.8	469.5 ± 33.7
	CEM I	324.5 ± 30.4	655.6 ± 162.8	534.6 ± 16.0	681.5 ± 13.0	703.5 ± 7.3
	CEM III	247.0 ± 1.4	436.4 ± 2.6	338.8 ± 3.0	425.1 ± 1.3	518.1 ± 6.5
	MKAA	168.0 ± 18.4	100.0 ± 0.1	68.5 ± 0.8	119.3 ± 13.7	166.2 ± 24.2
$[PO_4^{3-}]$	**Control**	26.7 ± 9.0	6.2 ± 0.3	15.2 ± 0.5	11.7 ± 8.5	14.3 ± 6.6
	CEM I	25.1 ± 3.7	4.6 ± 0.9	13.9 ± 0.8	14.3 ± 2.6	16.6 ± 2.0
	CEM III	22.5 ± 2.1	3.6 ± 1.1	11.9 ± 1.0	8.2 ± 5.7	16.7 ± 1.9
	MKAA	21.0 ± 3.5	4.2 ± 2.7	21.6 ± 2.0	24.6 ± 1.0	26.7 ± 1.9

$[Mg^{2+}]$	**Control**	2.2 ± 0.6	56.3 ± 3.5	32.6 ± 1.4	38.6 ± 4.2	38.3 ± 5.9
	CEM I	2.9 ± 1.3	56.7 ± 2.4	50.1 ± 7.8	55.6 ± 6.1	58.4 ± 3.5
	CEM III	2.8 ± 0.6	67.2 ± 2.5	65.3 ± 2.0	68.9 ± 4.8	65.7 ± 1.7
	MKAA	27.4 ± 2.9	45.3 ± 3.6	19.3 ± 1.6	19.9 ± 1.5	30.7 ± 2.6

In the bioreactors containing the cementitious materials and in the controls, the sodium concentration remained between 100 and 200 $mg.L^{-1}$ throughout the experiment. Because of its sodium activation, the MKAA released much more Na^+: its concentration in the bioreactor liquid phase increased until day 60 and remained around 2000 $mg.L^{-1}$ thereafter.

The potassium concentration followed the same trend in the bioreactors containing the cementitious materials and in the control bioreactors: a first increase until day 35 and slight variations thereafter. The potassium concentration in the control bioreactor was between 300 $mg.L^{-1}$ and 400 $mg.L^{-1}$ during the experiment. Bioreactors containing the cementitious materials showed higher potassium concentrations, between 300 $mg.L^{-1}$ and 700 $mg.L^{-1}$ in the bioreactor containing CEM I and between 250 $mg.L^{-1}$ and 500 $mg.L^{-1}$ in the bioreactors containing CEM III. The potassium concentration in the bioreactors containing MKAA remained between 100 and 200 $mg.L^{-1}$ throughout the experiment. Moreover, the K^+ concentration for the MKAA bioreactors was found to be lower than that of the control bioreactor during the whole experiment: the release of Na^+ could have led to an exchange of the Na^+ and the K^+ ions in the material (O'Connor et al., 2010).

The phosphate concentrations followed a similar trend in the control bioreactors and in the bioreactors containing CEM I and CEM III: a first decrease from 25 ± 2 $mg.L^{-1}$ to 5 ± 1 $mg.L^{-1}$ and then an increase leading to stable concentrations between 8 and 15 $mg.L^{-1}$. In the bioreactors containing MKAA, the phosphate concentration was similar to that in the other bioreactors during two cycles, but rose significantly afterwards (24 ± 3 $mg.L^{-1}$).

Magnesium is provided by the inoculum and by the leaching of the materials. In the control bioreactors and in the bioreactors containing CEM I and CEM III, the magnesium concentration started at about 3 $mg.L^{-1}$ and reached 60 ± 6 $mg.L^{-1}$ at the start of the second cycle. The magnesium concentration was then stable at about 36 $mg.L^{-1}$, 55 $mg.L^{-1}$ and 67 $mg.L^{-1}$ in the control bioreactor, the bioreactor containing CEM I and the bioreactor containing CEM III, respectively. The initial magnesium concentration (day 1) in the bioreactor containing MKAA was higher than in the others (27.4 ± 2.9 $mg.L^{-1}$) but the following increase was less significant than in the other bioreactors. The magnesium concentration then remained between 20 and 30 $mg.L^{-1}$.

3.2 Microstructural, chemical and mineralogical changes in the material samples

3.2.1 Microstructural changes

Figure 6 shows the images of the samples of materials obtained by SEM in back-scattered electron (BSE) mode before immersion and after the third and the fifth cycles. The surfaces in contact with the fermenting biowaste are at the top of the images and the cores of the specimens at the bottom. BSE images are characterized by a range of grey levels, which are proportional to the average atomic weight of the analysed volume (or density). Thus, the grey level gives information about the different phases, the heaviest elements being bright and the lightest elements being dark. The presence of a small quantity of solid (i.e. a high quantity of porosity) in an analysed area is characterized by a darker contrast.

After the immersion, the cores of the specimens showed a high density of anhydrous residual grains (lighter grey grains). The outer layer (in contact with the biowaste) showed darker grey zones, corresponding to a decrease of mass density following the exposure to the fermenting biowaste. Most of the cracks observed were probably linked to shrinkage caused by sample preparation and to the more fragile nature of the external zones. The CEM I paste already showed a lower density zone after 3 cycles and a local dissolution was observed after the 5^{th} cycle (top right of the image). This dissolution may have been associated with high local concentrations of acid.

After the 3rd cycle, the CEM III paste showed cracks, probably due to the way the sample was prepared. However, after the 5th cycle, no dissolution was observed but a zone of lower density appeared in the external part.

In contrast, the MKAA paste did not show any sign of deterioration after 3 cycles and only a thin layer on the external part presented a lower density after 5 cycles.

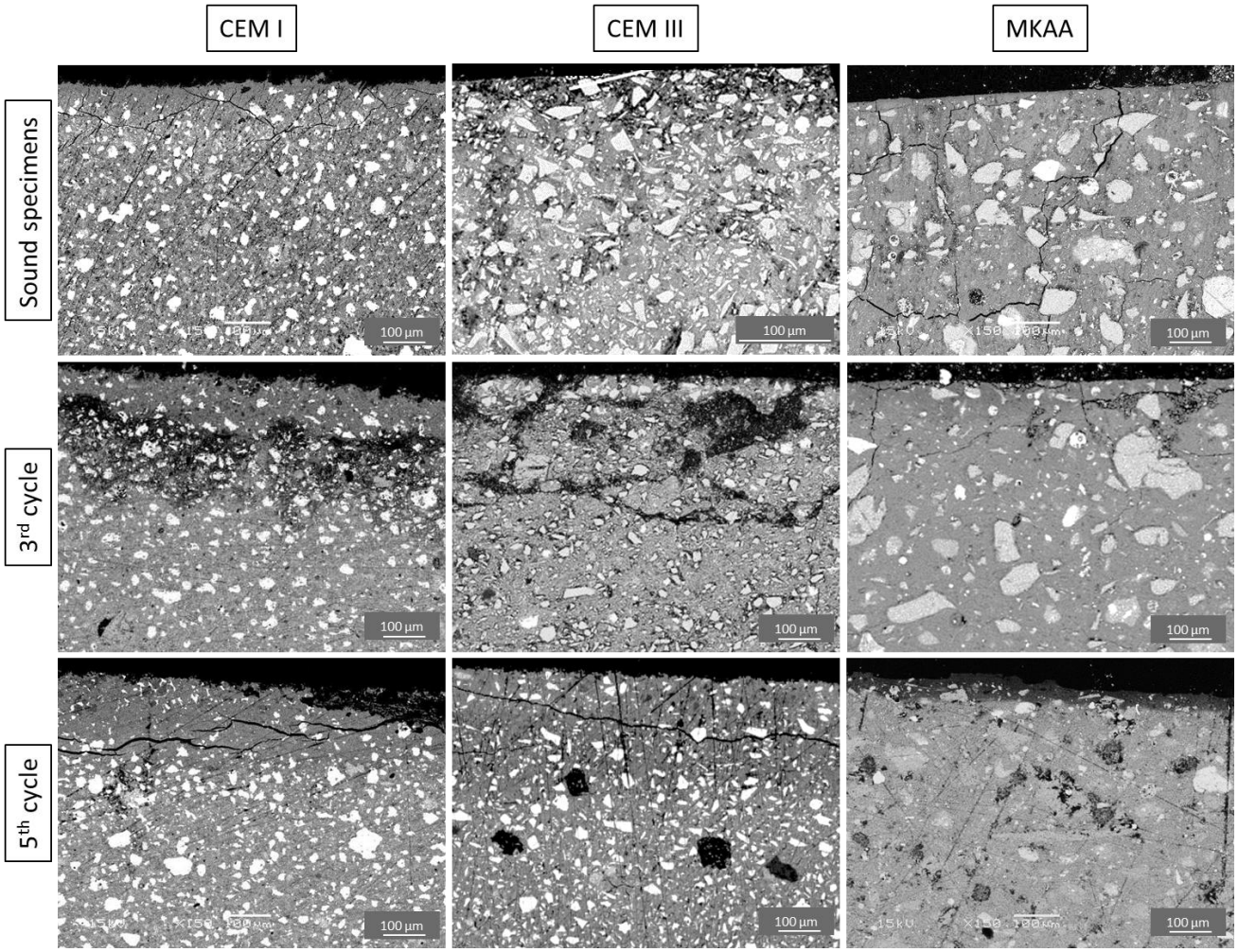

Figure 6: Observation of the paste by scanning electronic microscopy in back-scattered electron mode, before immersion and after the third and fifth cycles. Surface in contact with the fermenting biowaste is at the top of each image and the core of the specimen is at the bottom.

3.2.2 *Chemical and mineralogical changes*

Chemical composition profiles (EPMA), microscopic observations (SEM in BSE mode) and XRD analyses were carried out to identify the structural, chemical and mineralogical changes after the 3rd cycle for the CEM I (Figure 7) and CEM III pastes (Figure 8).

3.2.2.1 CEM I and CEM III

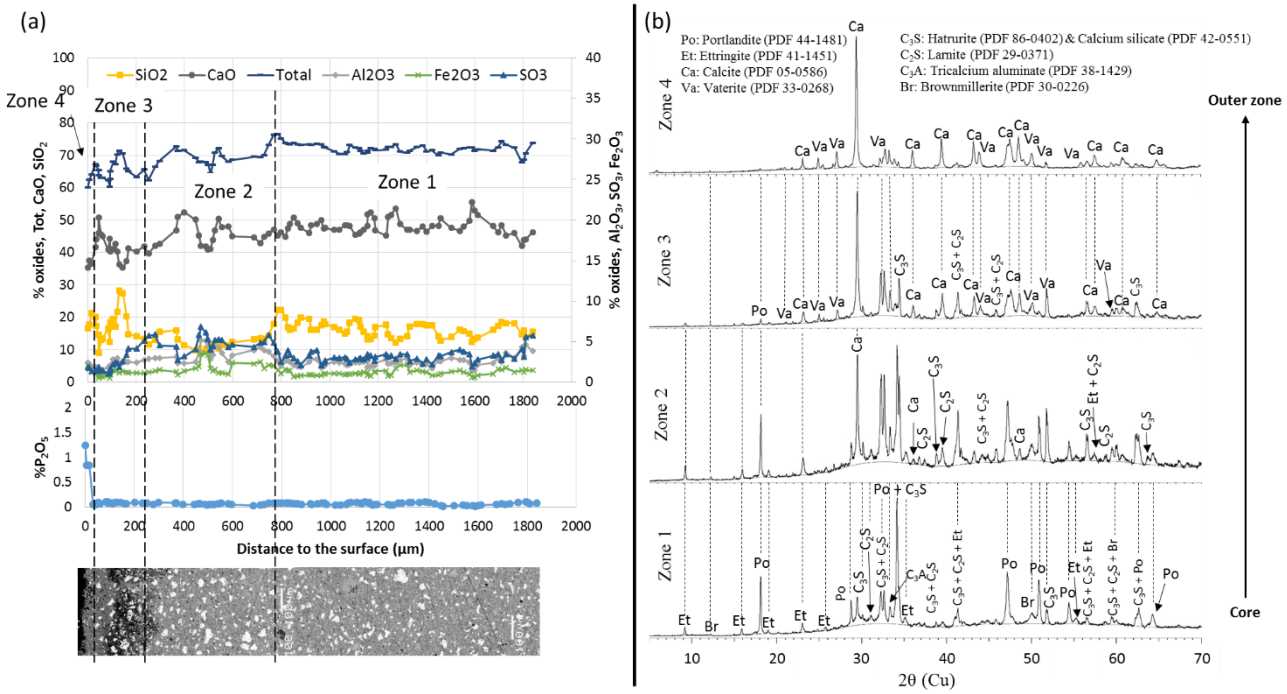

Figure 7: (a) Chemical composition profile, according to the distance to the surface, of a CEM I paste immersed in the liquid phase in anaerobic digestion conditions (EPMA), and SEM observations of the polished sections in BSE mode. (b) Mineralogical analyses of the same sample immersed for three consecutive cycles

Zonation, from the core to the outer layer, was identified for the sample and is represented in the chemical composition profile (zones 1 to 4):

Zone 1 corresponds to the sound zone. The SEM images show unaltered cement pastes where white anhydrous grains are surrounded by the hydrated paste. Pastes are predominantly composed of calcium and silicon, with minor amounts of aluminium, sulfur and iron. The mineralogical analyses show peaks of hydrated phases and anhydrous phases: portlandite, ettringite, C_2S, C_3S and C_4AF, and also merwinite C_3MS_2 for the CEM III paste.

Zone 2 is 400 µm thick and shows an enrichment in sulfur. The relative silica content drops in this zone whereas the aluminium content increases. The slight intensification of the ettringite peaks in the mineralogical patterns suggests that, as in the study by Voegel et al. (2016), the sulfur enrichment could come from the precipitation of secondary ettringite in this zone. This secondary ettringite precipitation is classically observed in transition zones of specimens exposed to leaching because of the diffusion of sulfates from the altered zone (Bertron et al., 2005a; Faucon et al., 1998). The total oxide content remains stable.

Zone 3, the thickness of which is about 400 µm in the CEM I paste and 180 µm in the CEM III paste, is first marked by a decrease in the calcium and sulfur contents. The total oxides content decreases as a result of the decrease of CaO. In this zone, the SEM image shows a very low density and a heterogeneous layer. The mineralogical patterns show the precipitation of calcium carbonates, calcite and vaterite, with a decrease of the peak intensities in the initial phases. This suggests combined dissolution/precipitation phenomena.

Zone 4, about 30 µm thick, is marked by a sudden increase of the phosphorus content - from 0 to 1.25% in the CEM I paste and from 0 to 1% in the CEM III paste. This zone also shows a decrease in the CaO, SiO_2 and total oxides contents. After the third cycle, the only remaining crystallized phases are the calcium carbonates, calcite and vaterite.

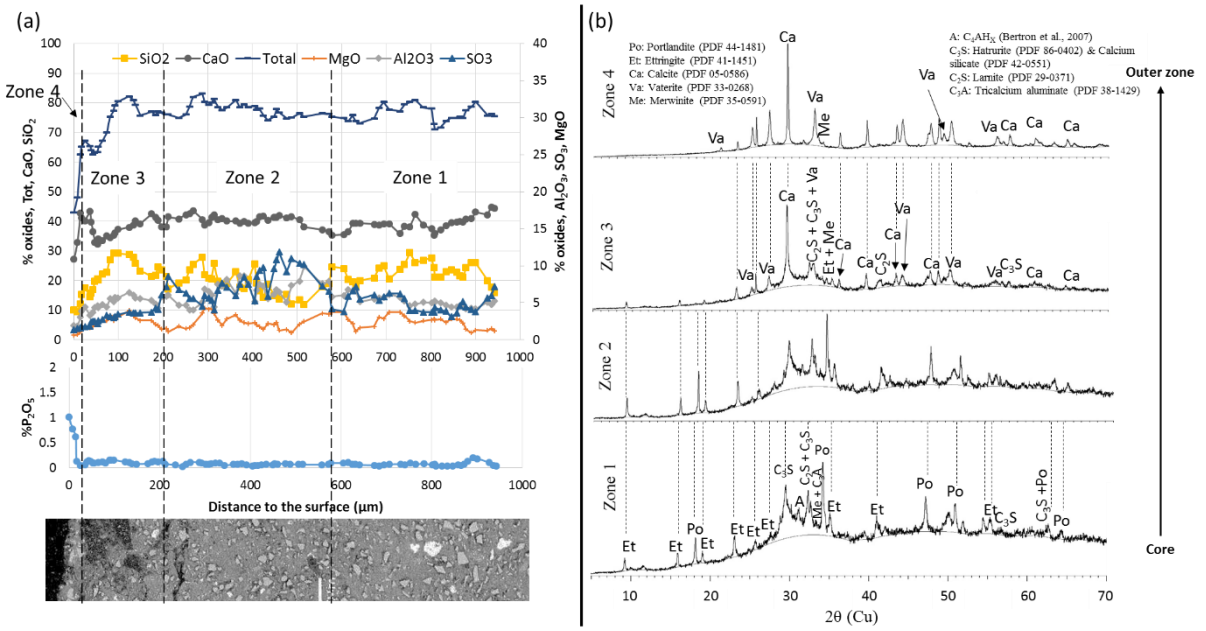

Figure 8: (a) Chemical composition profile, according to the distance to the surface, of a CEM III paste immersed in the liquid phase in anaerobic digestion conditions (EPMA), and SEM observations of the polished sections in BSE mode. (b) Mineralogical analyses of the same sample immersed for three consecutive cycles

3.2.2.2 MKAA

The chemical composition of the MKAA specimen after the third cycle is presented in Figure 9. The specimen did not seem to present degradation at any stage of the experiment, except on a thin outer layer (50 µm after the third cycle), which was darker on the SEM image: the release of alkaline ions did not impact the major oxides over more than 50 µm.

The XRD analyses after the third cycle were identical to the initial XRD analyses of the sound paste. The crystallized phases were mainly quartz but hematite, calcite, anatase and mullite were also present. Their analyses through time did not highlight any mineralogical change between the core of the specimen and the outer zone. However, it should be noted that the mainly amorphous nature of the sound MKAA paste did not allow every mineralogical change to be identified.

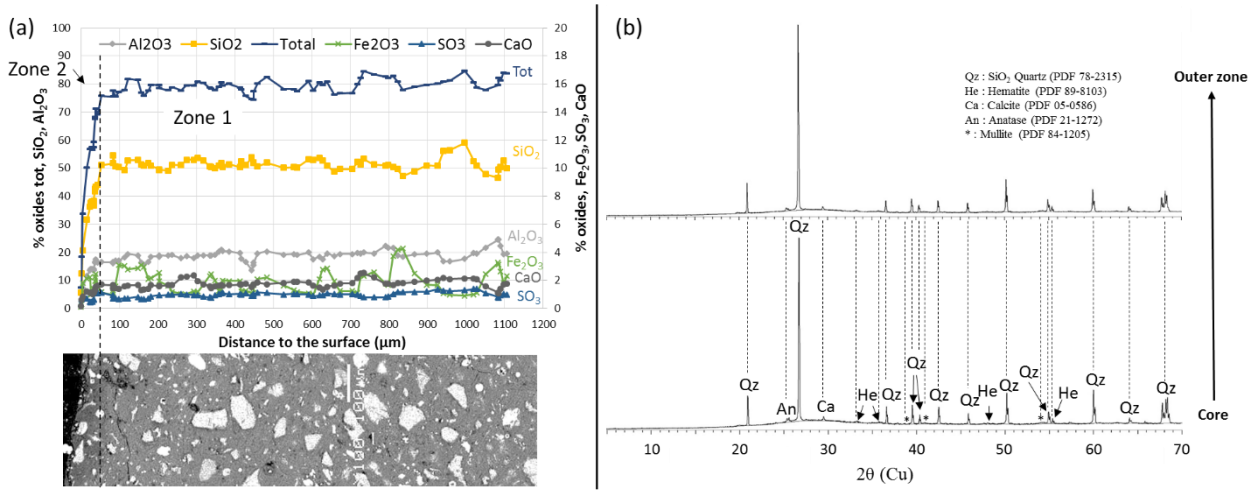

Figure 9: (a) Chemical composition profile according to the distance to the surface (EPMA) of an MKAA paste immersed in the liquid phase in anaerobic digestion conditions), and SEM observations of the polished sections in BSE mode. (b) Mineralogical analyses of the same sample immersed for three consecutive cycles

4 Discussion

4.1 Characteristics of the digestate as a function of the material nature during anaerobic digestion

4.1.1 Production of biogas and volatile fatty acids

Correlations of the biogas production, the VFA production and the pH of each type of bioreactor were investigated to understand the effect of the nature of each sample on the anaerobic digestion process: the presence of materials had an impact on the digestion but it was limited in time. In the short term, two types of behaviour were identified:

- In the bioreactors containing CEM I and CEM III, the VFA were not well consumed and accumulated in the liquid environment during the first cycle but biogas was still produced.
- In the bioreactors containing MKAA, the material presence had a strong impact on the liquid environment for three cycles since the VFA accumulated first and no biogas was produced during two cycles.

For the control bioreactors, the first cycle showed an acidification of the media from a pH of 8.38 up to 7.12, corresponding to VFA production (hydrolysis and acidogenesis steps) (Han et al., 2019). It can be noticed that the initial value of the pH was much higher than the ones reported by Han et al. (2019) and Yun et al. (2018), respectively 6.7 and 6.1. According to Yun et al. (2018), this low pH comes from the partial acid peculiarity of the cattle manure. In the current study, since the cattle manure was not fresh, the substrate acids were probably already consumed. Moreover, the inoculum used was adapted to the substrate and was rich in bicarbonates, which explains the higher pH. A maximum VFA concentration of 0.35 g.L-1 was reached and the VFA were then well consumed by the microorganisms: after the thirteenth day, the total acid concentration decreased and biogas was produced, meaning that the anaerobic digestion process was complete. This effective digestion of the substrate continued through the following cycles with a pH that remained stable between 7.3 and 7.8, which is slightly lower but coherent with the pH values of the control check sample of Han et al. (2019).

The bioreactors containing CEM I and CEM III pastes underwent a pH increase in the first three days due to the alkaline nature of the materials, which released alkaline ions during the first cycle. Afterwards, the pH decreased while the VFA concentration increased over a period of 10 days. The increase in VFA concentration was slower and less significant in these bioreactors than in the control ones (maximum VFA concentration of 0.26 $g.L^{-1}$and 0.29 $g.L^{-1}$ in the bioreactors containing CEM I and CEM III respectively). From day 13, a slow consumption of the acids by the methanogenic archaea occurred, highlighted by a decrease of the VFA concentration. The lack of efficiency in the VFA production and consumption was associated with a low production of biogas during the first cycle. During the second cycle, the bioreactors containing cementitious materials reached a pH about 7.5, which was similar to that of the control bioreactors and suitable for anaerobic digestion - especially the methanogenic microbial activities, for which the optimal pH range is between 6.5 and 8.2 (Kothari et al., 2014). During this cycle, the bioreactors containing the cementitious materials produced biogas in greater quantities than the control ones did, due to the undigested cattle manure

491 remaining after the first cycle. From the third cycle, these bioreactors behaved similarly to the
492 controls and the presence of materials no longer disturbed the anaerobic digestion process.

493 The lower VFA production of the first cycle in the bioreactors containing cementitious materials was
494 also observed by Voegel et al. (2016). In their study, CEM I pastes (water/cement = 0.4) were
495 immersed in an inoculated synthetic biowaste, representative of organic domestic waste, for a single
496 cycle of anaerobic digestion. The substrate induced significantly higher maximum acid concentrations
497 than in the current study, about 2.90 $g.L^{-1}$ (43 $mmol.L^{-1}$) in the control bioreactors and a slightly lower
498 concentration, about 2.85 $g.L^{-1}$ (41 $mmol.L^{-1}$), in the bioreactors containing CEM I paste. Moreover,
499 the pH values between 7 and 8 found in the studies by Voegel et al. (2019b, 2016) were similar to
500 those encountered in the current study, whereas a slightly lower pH, around 7, was observed in the
501 liquid phase of a laboratory fermenter in a study by Koenig and Dehn (2016).

502 In the MKAA bioreactors, the pH was very high, between 9 and 9.5, during the first two cycles. This
503 can be explained by the strong release of alkalis that occurred during the first cycle (about 2 g/L of
504 Na^+, Table 3). These high pH values were much higher than the ones tolerated by the methanogenic
505 archaea (optimal pH around 7 (Chae et al., 2010)). These are the most fragile microorganisms of the
506 anaerobic digestion process and are sensitive to pH variations (Chae et al., 2010), unsuitable pH
507 leading to very low biogas production. At the same time, the VFA accumulated in the medium and
508 accentuated the environment's aggressiveness. The formation of VFA in the medium showed that
509 the high pH did not disturb the first steps of the anaerobic digestion (hydrolysis, acidogenesis),
510 although the optimal operating pH of these bacteria is between 5.5 and 6.5 (Hagos et al., 2017; Han
511 et al., 2016; J. Kim et al., 2003; M. Kim et al., 2003; Yu and Fang, 2002). The third cycle showed a
512 decrease of the pH, probably due to the accumulation of the VFA in the medium, since most alkalis
513 were released during the first cycle. This decrease of pH allowed the methanogenic activities to take
514 place, and thus the rapid consumption of the VFA, leading to a significant production of biogas. The

accumulation of methane produced during the third cycle indicated that not all the methane potential was expressed earlier, due to the delay in the anaerobic digestion reactions.

According to the thermochemical equilibria (Reactions 1 and 2) associated with Henry's law at 35°C, the increase in pH during the first cycles in the bioreactors containing materials led to a reduction of the volatilization potential of CO_2, which can explain the lower CO_2 amount in the gas phase during this period.

In all the bioreactors containing materials, when conditions suited to anaerobic digestion were well established, the process remained efficient over time. Moreover, the final total production of methane was equivalent in all the bioreactors (Figure 2), so the presence of the materials nevertheless allowed the expression of the methane potential of the entire amount of substrate. It can be assumed that the retarding effect of the MKAA on the biogas production is only expressed in the short term, as geopolymers rapidly lose their alkaline charge, which is mainly present in the liquid contained inside pores (Khan et al., 2020).

4.1.2 Ammonium production

A significant difference of ammonium concentration was observed between, on the one hand, the control bioreactors and the bioreactors containing the cementitious materials and, on the other hand, the bioreactors containing MKAA. This suggests a specific behaviour of the MKAA towards ammonium, which needs to be studied more thoroughly.

4.1.2.1 Control bioreactors and bioreactors containing CEM I and CEM III

The ammonium concentrations in the CEM I, CEM III and control bioreactors increased until a maximum of about 750 $mg.L^{-1}$ was reached on the 35^{th} day. Similar concentrations were found in Voegel et al.'s study (2016) (800 $mg.L^{-1}$), where the presence of CEM I cement paste also did not influence the ammonium production. It could be expected that each addition of cattle manure would lead to an increase in the potential of hydrolysable nitrogen but the ammonium concentrations

539 actually decreased during the experiment, meaning that this element was mainly brought by the
540 inoculum. In Voegel et al. (2019b), the ammonium concentration did not increase with a new
541 substrate addition either, since the measured concentrations were 988 $mg.L^{-1}$ (54.9 $mmol.L^{-1}$) in the
542 first cycle and 940 $mg.L^{-1}$ (52.24 $mmol.L^{-1}$) in the second. The decrease of the ammonium
543 concentration could be explained by several phenomena: nitrogen consumption by bacteria for
544 growth (Kuypers et al., 2018), stripping of the ammonium in the gas phase in the form of ammonia
545 (Limoli et al., 2016), and/or formation of precipitates containing ammonium (struvite, for example)
546 (Cerrillo et al., 2015; Escudero et al., 2015).

547 Using the chemical oxygen demand (COD) of the CH_4 production with the biomass production yields
548 proposed by the Anaerobic Digestion Model n° 1 (ADM1) (Batstone et al., 2002), the quantity of
549 biomass produced per cycle was estimated and its growth only required 61 mg of nitrogen, which is
550 insufficient to justify the difference of 253 mg of nitrogen lost between the maximum concentrations
551 (day 37) and the end of the fifth cycle.

552 The method used for gas chromatography did not allow identifying and measuring ammonia in the
553 gas phase. Thus, the thermochemical equilibrium (Reaction 4) associated with Henry's law at 35°C
554 and atmospheric pressure, were used and it was found that the amount of volatile ammonia passing
555 into the gas phase did not exceed 0.15 mg for the whole experiment in these bioreactors.

$$NH_4^+ + H_2O \rightleftharpoons NH_3 + H_3O^+ : \mathrm{pKa} = 9.25 \quad (4)$$

556 Moreover, thermodynamic calculations using the geochemical code PHREEQC and considering the
557 temperature, the pH and the concentrations in the solution (N as ammonium, P as phosphate, K, Mg,
558 Cl, Ca, Na, inorganic carbon) (Table 3) were carried out to assess the possibility of struvite
559 precipitation during the digestion. The MINTEQ database was used together with the struvite
560 solubility value at 35°C; $pK_{sp\ struvite}$= -13.20 (Bhuiyan et al., 2007). Figure 10 shows the variation of the
561 struvite saturation index of the liquid phase of the bioreactors containing CEM I and MKAA with time.
562 Precipitation conditions are met for a positive index, while a negative index corresponds to

dissolution if struvite is present. The bioreactors containing CEM I were chosen to represent the bioreactors containing CEM I and CEM III and the control bioreactors. In these bioreactors, struvite precipitation was continuously possible during the experiment, with higher indices in the first cycle and values closer to 0 at the end of the experiment. The ammonium loss during the experiment could thus be explained by the precipitation of struvite.

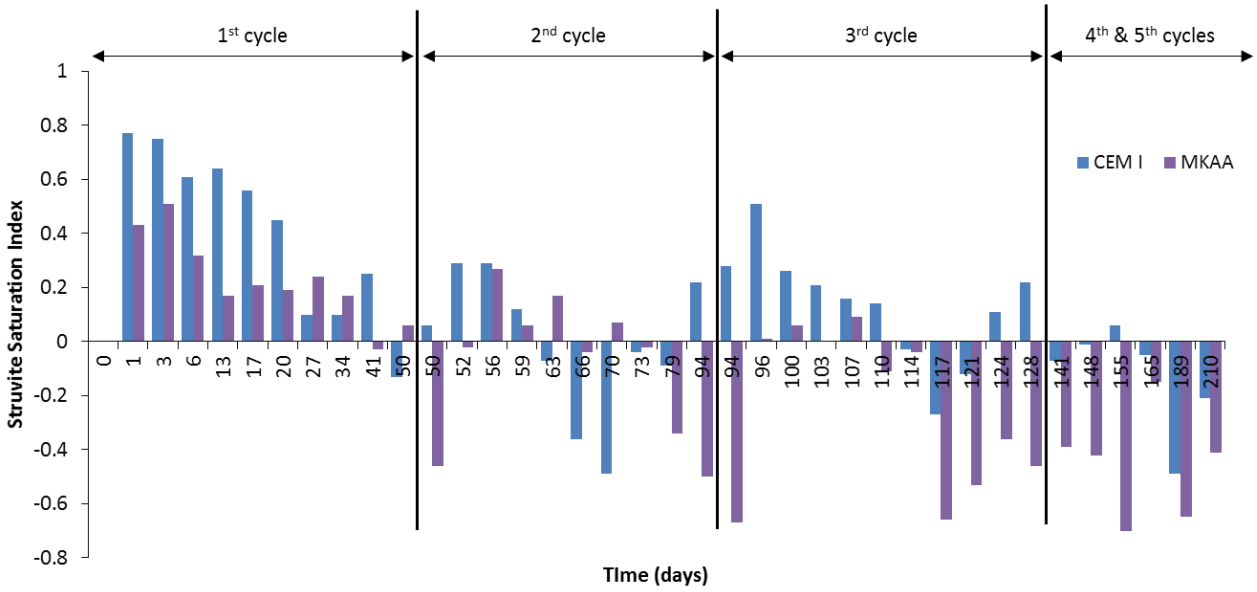

Figure 10: Variation with time of the Struvite Saturation Index of the liquid phase of the bioreactors containing CEM I and MKAA

4.1.2.2 Bioreactors containing MKAA

In comparison with the other bioreactors, the bioreactors containing MKAA reached a lower maximum ammonium concentration, of about 400 $mg.L^{-1}$, on day 30. At this stage of the process, the pH was about 9.5. According to the pKa of the acid and conjugate base NH_4^+/NH_3, i.e. 9.25 (Reaction 4), the ammonium was thus present in the form of both ammonium and ammonia. The volatile ammonia form could have passed into the gas phase, leading to a weaker ammonium concentration measured in the liquid phase of the MKAA bioreactors. Nevertheless, this hypothesis implies that a fall in pH should lead to an increase in the ammonium concentration in the liquid medium, whereas the concentration actually dropped quickly during the second cycle, at the same time as the pH

started decreasing. Moreover, the thermochemical equilibrium (Reaction 4) associated with Henry's law at 35°C and atmospheric pressure allowed the amount of ammonia in the gas phase to be calculated: this amount was very small throughout the experiment and did not exceed 0.5 mg of NH_3, which does not explain the lower ammonium concentration found in the liquid phase of the MKAA bioreactors.

The thermodynamic calculations using the geochemical code PHREEQC allowed us to follow the variation of the Struvite Saturation Index of the liquid phase of the bioreactors containing MKAA (Figure 10). The index was positive during the first cycle, but with lower values than in the other bioreactors, while the ammonium concentration was lower in the bioreactors containing MKAA. Moreover, whereas the acidification of the environment (from day 66) led to negative or neutral struvite saturation indices, the ammonium concentration decreased in the bioreactors containing MKAA. Thus, even if struvite can precipitate at the beginning of the experiment, the trend of the ammonium concentration in the bioreactors containing MKAA remains unexplained, and is probably the result of a combination of phenomena.

According to the literature, natural zeolites (hydrated aluminosilicates) have been successfully used in wastewater treatment to remove ammonium (Luukkonen et al., 2016; Wang et al., 2011). The ion exchange properties of the material are attributed to the charge-balancing cation (Na^+ or K^+) being replaced by another cation, such as K^+, Ag^+, NH_4^+ or Pb^{2+} (O'Connor et al., 2010). As synthetic zeolites, metakaolin-based alkali-activated geopolymers have been studied for ammonium removal by Luukkonen et al. (2016). In this study, the maximum capacity of metakaolin geopolymer to remove NH_4^+ was 46% higher than that of natural zeolite, showing its potential interest in such an application. The adsorption process is influenced by the pH: for pH higher than 9.25, NH_4^+ deprotonates to NH_3 (Reaction 4) which is not favourable to adsorption. Actually, the ammonium adsorption capacity seems to decrease even from pH ≥7 (Marañón et al., 2006).

According to the former results, it is thus possible that ammonium was adsorbed on the surface of the MKAA pastes through an exchange mechanism between a cation of the sound paste and the NH_4^+ cation in the liquid phase. The liquid medium analyses showed high concentrations of Na^+ (2000 $mg.L^{-1}$ on average), this element being leached from the MKAA matrix. The drop of ammonium concentration during the second cycle might be explained by the sudden drop of pH (due to the VFA accumulation) leading to more suitable adsorption conditions. Then, although the ammonium concentration appeared to be lower in the bioreactors containing MKAA, the production of ammonium in the liquid medium due to digestion was probably similar in all the bioreactors, the difference being adsorbed by the MKAA.

4.2 Exchange phenomena between the MKAA and NH_4^+

In order to investigate the assumption concerning the adsorption of NH_4^+ by the MKAA, based on the literature, an additional test was carried out to study the interaction between the MKAA and the NH_4^+ cation. The test design was adapted from the experimental protocols implemented by Lin et al. (2013) and Luukkonen et al. (2016).

This experiment aimed (i) to investigate the exchange phenomena between the MKAA and NH_4^+ for different pH values and (ii) to understand how the ammonium cation interacted with the material. To this end, MKAA powder was immersed in an ammonium nitrate solution and the ammonium concentration was monitored for various pH values. The remaining MKAA powder was also analysed.

4.2.1 Experimental protocol

An 800 $mg.L^{-1}$ (0.0444 $mol.L^{-1}$) ammonium nitrate solution was prepared with demineralized water (according to the ammonium concentration found in the control bioreactors) and a cylindrical specimen of MKAA paste (75 mm high and 35 mm in diameter) was ground to 80 µm using a disc mill.

500 mL of solution was poured into a glass reactor thermostatically controlled at 35°C with magnetic stirring (Annexe A). The pH value was measured continuously and recorded every 15 seconds. After about 30 minutes (the time for the temperature of the ammonium nitrate solution to reach 35°C), 10 g of MKAA powder was poured into the reactor. After 3 hours, 1 mL of concentrated HNO_3 acid (69%) was added in order to lower the pH. Samples of the liquid were then taken at different stages of the experiment to be analysed by Ion Chromatography (Thermo Electron ICS 300, CS16 column). The pH evolution and the distribution of the liquid samples in time (W1 to W5) are presented in Figure 11 (a). The experiment was performed in duplicate (reactor 1 and reactor 2). In order to reach another final pH, a supplementary experiment was run with the addition of 350 µL of HNO_3 only. The pH evolution and the distribution of the liquid samples S1 & S2 in time are presented in Figure 11 (b).

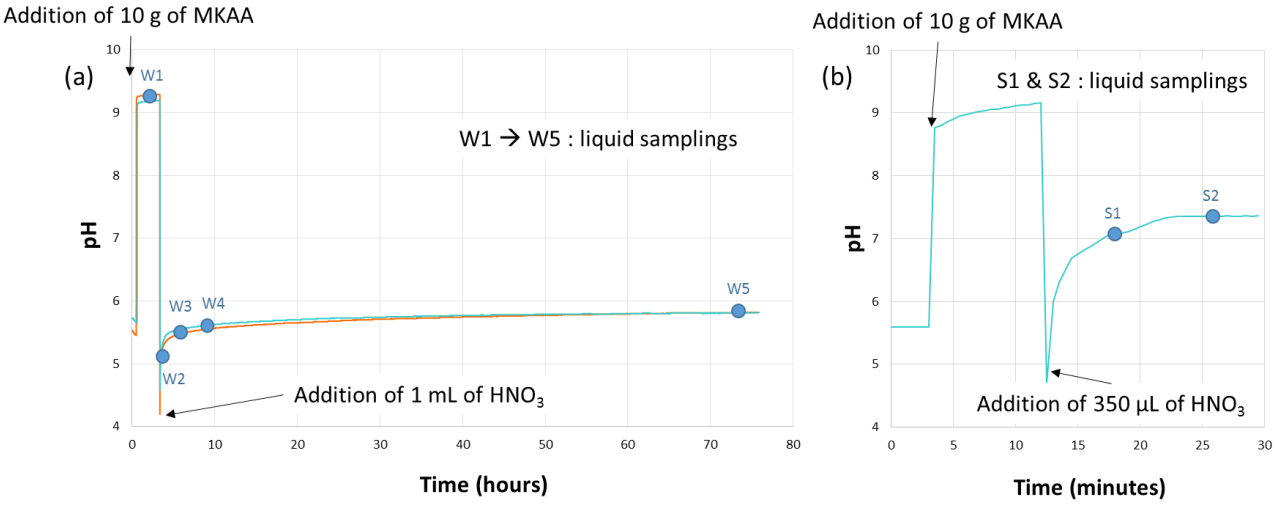

Figure 11: pH evolution according to time and distribution in time of the liquid sampling: (a) in the two duplicate reactors for 1 mL of added HNO_3 and (b) in the solution of the supplementary experiment for 350 µL of added HNO_3

After the end of the main experiment, the solution was centrifuged in order to collect the MKAA powder. It was then immersed in isopropanol for 15 minutes to dry by solvent exchange (Scrivener et al., 2016; Snellings et al., 2018). After another centrifugation, the powder was collected and placed in a vacuum desiccator for 1 hour to finish drying. This powder and a control MKAA powder were analysed in several ways: thermogravimetric analysis (NETZSCH STA 449F3); ^{27}Al, ^{29}Si and ^{1}H nuclear magnetic resonance (NMR) (Brucker Avance 4000 III HD MAS); and infrared spectrometry (FTIR)

(Perkin-Elmer Spectrum). No significant differences were observed in the ^{27}Al and ^{29}Si NMR spectra between the control MKAA powder and the powder from the experiment (called MKAA – NH_4^+ powder), and these results are not presented.

4.2.2 Liquid analysis

The ammonium concentration [NH_4^+] was measured by Ion Chromatography and the results from reactor 1 and the supplementary experiment are presented in Table 4. These analyses highlighted an exchange mechanism between the MKAA and the ammonium solution since the measured concentrations were different from the initial ammonium concentration of the solution (800 mg.L^{-1}). When the MKAA powder was added, the pH increased to 9.29 and the ammonium concentration decreased from 800 mg.L^{-1} to 437.9 mg.L^{-1}. The pH decrease from 9.29 to 7.06 led to a decrease of the ammonium concentration to 351.1 mg.L^{-1}. From then on, the ammonium concentration increased when the pH was decreased, but still remained below 800 mg.L^{-1}.

Table 4: Ammonium concentration of the liquid withdrawals according to the pH, in mg.L^{-1}

Samples	*W1*	*S2*	*S1*	*W5*	*W4*	*W3*	*W2*
Decreasing pH	9.29	7.36	7.06	5.82	5.52	5.49	5.29
[NH_4^+]	437.9	357.9	351.1	520.4	525.3	530.1	530.0

4.2.3 MKAA powder analyses

Differential Thermo Gravimetry (DTG), ^1H NMR and FTIR analyses of the control MKAA powder and the powder from the reactor 1 are presented in Figure 12 (a), (b) and (c) respectively.

Figure 12 (a) shows that, despite the drying by solvent exchange, the MKAA – NH_4^+ powder contained more free water than the control powder (intense peak at 143°C). The DTG analysis differed slightly with a weak, broad peak centred on 318°C in the MKAA – NH_4^+ powder, which could be correlated with the thermal decomposition of the NH_4^+ cation identified in two different clays at 327°C and

330°C by Gautier et al. (2010) and Yariv (1985), respectively. Some calcium carbonates were identified by a bump at 670°C (Wianglor et al., 2017) in the control MKAA powder.

Figure 12 (b) shows a fine, intense peak for both specimens at 0.94 ppm, which corresponds to the SiOH group usually found between 1 and 2.2 ppm in the literature (Hunger, 1996; O'Connor et al., 2010). All the peaks between 3.5 and 4.9 were associated with water and, more precisely for hydrated Na-form zeolites, with physisorbed water molecules (Hunger, 1996; O'Connor et al., 2010). Finally, a peak was detected in the MKAA – NH_4^+ powder only at 6.82 ppm and corresponded to the ammonium cation, whose signal appears between 6.5 and 7 ppm (Jacobs et al., 1993; O'Connor et al., 2010).

In addition to the peaks associated with water (3500 and 1640 cm^{-1}) (Ahmed et al., 2018; Aredes et al., 2015; Wang et al., 2005), the silicates (992 cm^{-1}) (O'Connor et al., 2010) and the carbonates (867 cm^{-1}), peaks centred on 3190 cm^{-1} and 1400 cm^{-1} can be seen in Figure 12 (c) and correspond to the ammonium cation (Mookherjee et al., 2005).

Thus, the analyses of the materials showed that ammonium from the solution was indeed exchanged towards the MKAA.

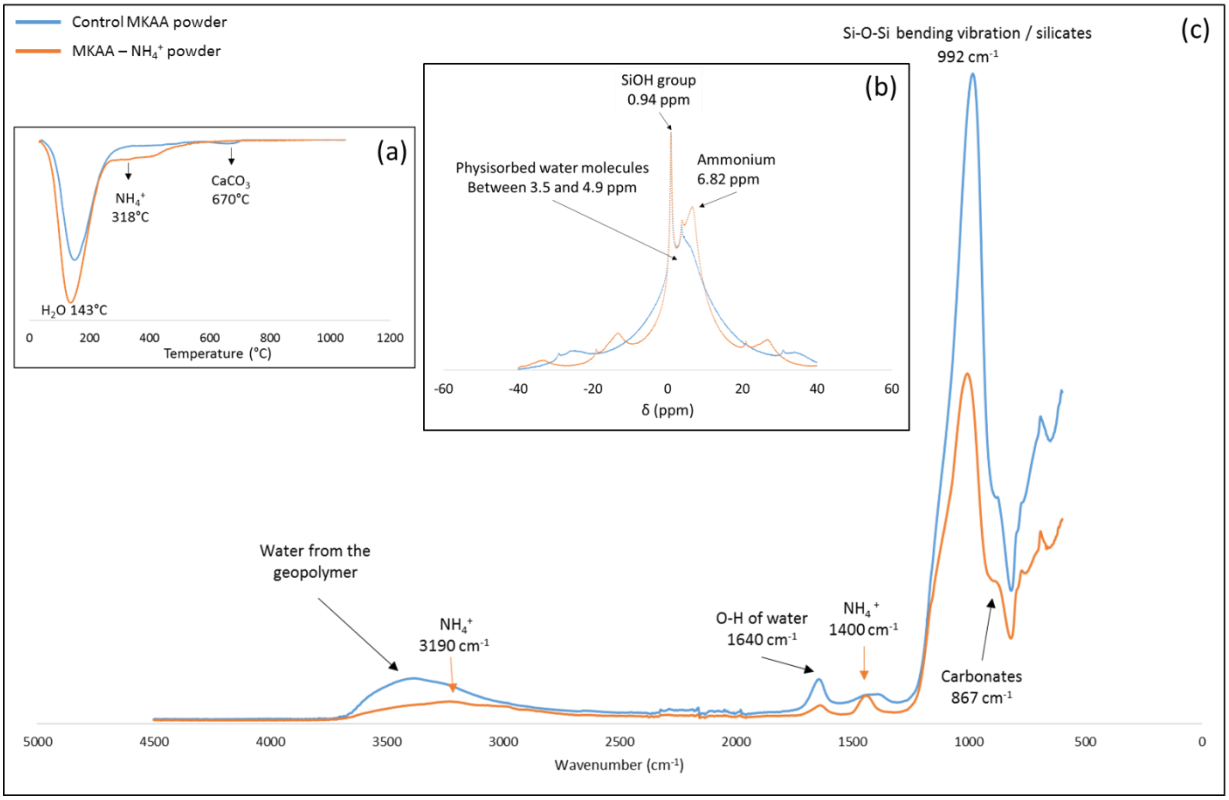

Figure 12: (a) Differential thermogravimetry, (b) ^{1}H Nuclear Magnetic Resonance, and (c) Fourier Transform Infrared Spectroscopy analyses of the control MKAA powder and the powder from the experiment (MKAA – NH_4^+). The main peaks are identified.

4.2.4 Exchange phenomena conclusions

In light of the previous results, it can be concluded that exchange phenomena between MKAA and NH_4^+ do exist. More precisely, the liquid analysis showed that the efficiency of this exchange depended on the pH, with a much greater transfer of ammonium to the MKAA when the pH was around 7. Moreover, the analyses of the MKAA powders confirmed the presence of the ammonium cation in the material, but without changing the Si-Al structure of the geopolymer. The nature of this exchange phenomenon would therefore be adsorption. Only 10 g of material was inserted in 500 mL of a 800 $mg.L^{-1}$ nitrate ammonium solution, whereas the cylinders immersed in the bioreactors are about 100 g for 800 mL of solution (ammonium in similar concentration, about 750 $mg.L^{-1}$). Even though the exchange surface is much higher in the case of a powdered material, the monolithic

samples of MKAA constituted, in theory, a sufficient source of exchange that could explain the lower ammonium concentrations found in the bioreactors containing MKAA.

4.3 Deterioration of the material samples

4.3.1 CEM I and CEM III

The chemical composition analysed in this study can be compared with results from previous studies. Voegel (2017) studied the biodeterioration phenomena of cementitious paste (water/cement = 0.40) in the submerged part of a digester with a laboratory test using typical food biowaste (solid/liquid ratio=224 $cm^2.L^{-1}$). After chemical and mineralogical tests, a zonation was established and phenomena were highlighted.

The chemical profiles were correlated with mineralogical changes and the CEM I and CEM III paste zonations were as follows:

- A sound zone at depth, corresponding to Zone 1, composed of the crystalline phases commonly found in the CEM I and CEM III matrices.
- A decrease in the CaO content and an enrichment in sulfur in Zone 2, probably correlated with the precipitation of secondary ettringite.
- Variations in the CaO content in Zone 3 and a slight decalcification, together with the precipitation of $CaCO_3$.
- A peak of phosphorus and decalcification of the matrix in Zone 4

From a mineralogical point of view, the X-Ray patterns obtained in the different zones of the CEM I and CEM III pastes after the third cycle showed leaching and carbonation phenomena: the initial phases (ettringite, portlandite, brownmillerite, C_3S and C_2S) were dissolved and calcium carbonates (calcite and vaterite) precipitated.

These main findings are in accordance with the results obtained by Bertron et al. (2017), where the authors sum up results on CEM I and CEM III from Voegel's study (2017). In addition, a fifth zone was found in Voegel's studies, which presents almost complete decalcification and the complete dissolution of hydrates and anhydrous phases, leading to an amorphous gel of silicon and aluminium.

The values from Table 2 allowed the inorganic carbon contents (H_2CO_3, HCO_3^- and CO_3^{2-} forms) in the liquid medium to be calculated at the end of each cycle. Most of the values were between 1000 and 2000 $mg.L^{-1}$ in the control bioreactors and in the bioreactors containing CEM I and CEM III. They were much higher than the values found by Voegel et al. (2019b, 2016) (about 140 $mg.L^{-1}$ or 2.3 $mmol.L^{-1}$) who used a different digestate that initially contained less dissolved CO_2, but were consistent with the concentrations of between 2000 and 3000 $mg.L^{-1}$ found in industrial digesters (McCarty, 1964). Moreover, the inorganic carbon content being strongly dependent on the pH and the rate of CO_2 in the gas phase, higher concentrations could be encountered in the medium during the digestion cycle, when the pH is higher or when the proportion of methane is smaller and that of CO_2 is larger. These high values accounted for the carbonation of the CEM I and CEM III samples. The presence of vaterite in the external part could be explained by the presence of highly decalcified C-S-H with low Ca/Si ratio (Morandeau et al., 2014). However, it could also be linked to the lower pH of the external zone since the crystallization of vaterite is predominant for pH<10 (Oral and Ercan, 2018; Tai and Chen, 1998). Moreover the experiment temperature of 35°C (close to 30°C) promotes the precipitation of both calcite and vaterite (Girou and Roques, 1971; Ševčík et al., 2015; Stepkowska et al., 2003; Wray and Daniels, 1956).

In the study by Koenig and Dehn (2016), in addition to calcium carbonates, struvite and quartz were detected in the surfaces of samples immersed in the liquid phase in a pilot scale fermenter. In the same study, vivianite, calcium-aluminium-iron-chloride-silicates, calcium-aluminium-iron oxides, ettringite and portlandite phases were measured on the near-surface area of samples immersed in

741 the laboratory. The presence of the initial phases portlandite and ettringite after 173 days of
742 immersion demonstrated low leaching of the materials.

743 After the third cycle, the same phenomena as in Voegel's study (2017) were detected for the CEM I
744 and CEM III samples, with equivalent degraded depths between the two materials. However, it can
745 be noted that, even with a longer exposure time in the cattle manure, the degradation of the
746 samples was less since the altered zone seemed to stop at zone 4, where the phosphorous peak was
747 found. This may have been due to (i) the different substrate used, which led to lower concentration
748 of aggressive agents, and/or (ii) the lower water/cement ratio of our matrices, leading to a reduction
749 of the porosity, influencing the transport mechanisms and reducing the specific surface area (Koenig
750 and Dehn, 2015).

751 *4.3.2 MKAA*

752 Even though the amorphous part of the material could not be characterized, the MKAA samples
753 seemed to show very stable behaviour with a small apparent degraded depth. However, the MKAA
754 released a large amount of alkalis at the start of the immersion, leading to a greater buffering
755 capacity compared to other binders: more than 90% of the water introduced was "free water"
756 (Pouhet et al., 2019) and contained a large amount of alkaline ions, which are easily released from
757 the paste via the porous network. This behaviour could be linked to the observations of Khan et al.
758 (2020), who studied the degradation of a fly ash (FA) based geopolymer mortar in a naturally
759 aggressive sewer environment. A mixture of sodium hydroxide solution and sodium silicate solution
760 was used as the activator. Although the geopolymer showed less degradation in terms of mass loss,
761 dry bulk density, compressive strength and surface disintegration compared to a Sulfate Resistant
762 (SR) ordinary Portland cement mortar, the geopolymer was also found to have a much greater
763 neutralization depth with a loss of alkalinity. This shows a greater penetration of the aggressive
764 agents and could be a concern for steel reinforced concrete. Moreover, the same geopolymer was
765 compared to an alkali-activated slag mortar (AASm) in another study (Khan et al., 2018) (same

766 activator) and the FA geopolymer showed much higher overall matrix deterioration than the AASm.
767 Nevertheless, the very different chemistries of the FA-based and AAS mortars do not allow a
768 qualitative comparison with the current study. In the study by Grengg et al. (2020), a metakaolin
769 similar to the one used in this study, which was quartz-rich, rust brown iron-rich (GP-K2) with
770 potassium silicate, was placed in a power main outlet storage basin heavily affected by MID in
771 Austria, together with a geopolymer made with high purity white metakaolin (GP-K1), a calcium
772 aluminate cement and a CEM I based material. Among these materials, after 18 months, the degree
773 of surface cracking and the estimated degradation rates were the lowest for the GP-K2 but highest
774 for the GP-K1. Thus, as pointed out by Grengg et al. (2020) and Khan et al. (2018), depending on the
775 design and the type of geopolymer, its resistance to bacteriological attacks in acid medium can vary
776 widely.

777 # 5 Conclusion

778 This study presented the exposure of three types of binder paste specimens to five consecutive
779 anaerobic digestion cycles of cattle manure in laboratory conditions, in an 8 months experiment. A
780 high solid/liquid ratio used for this study was chosen to exacerbate and evaluate the local interaction
781 mechanisms between the different materials and the anaerobic digestion medium.

782 The presence of the alkaline materials disrupted the efficiency of the anaerobic digestion process at
783 the local scale by slowing down the production and consumption of VFA and decreasing the
784 production of biogas. Whereas the Portland based materials, CEM I and CEM III pastes, impacted the
785 anaerobic digestion process for only one cycle, the alkali-activated materials (MKAA) released larger
786 amounts of alkalis at the start of the immersion, inducing a much higher pH, the VFA accumulation,
787 and almost no biogas production during the first two cycles. After 5 cycles, the final biogas
788 productions were equivalent for all the bioreactors and the anaerobic digestion process worked
789 under normal, efficient conditions. Thus, given the moderately aggressive conditions induced by the

liquid phase of anaerobic digestion, all materials can therefore be considered for construction application in such environment.

In terms of deterioration pattern the CEM I and CEM III biodeterioration were expressed by a combination of dissolution of the initial phases and decalcification on the surface, and precipitation of $CaCO_3$, in accordance with literature recent results. The original study of an alkali-activated geopolymer in an anaerobic digestion medium has revealed a very good behaviour of the material with very low degradations. In addition, the material was found to have interesting ammonium adsorption properties at the pH of the anaerobic digestion, significantly reducing the ammonium concentration in the liquid medium.

6 Acknowledgements

The authors gratefully thank the French National Research Agency (ANR) for funding the project BIBENdOM – ANR – 16 – CE22 – 001 DS0602. The authors also thank Evrard Mengelle, Simon Dubos, Mansour Bounouba and Chantha Kim for the pilot's design and the analytical support of the bioreactors.

Annexe

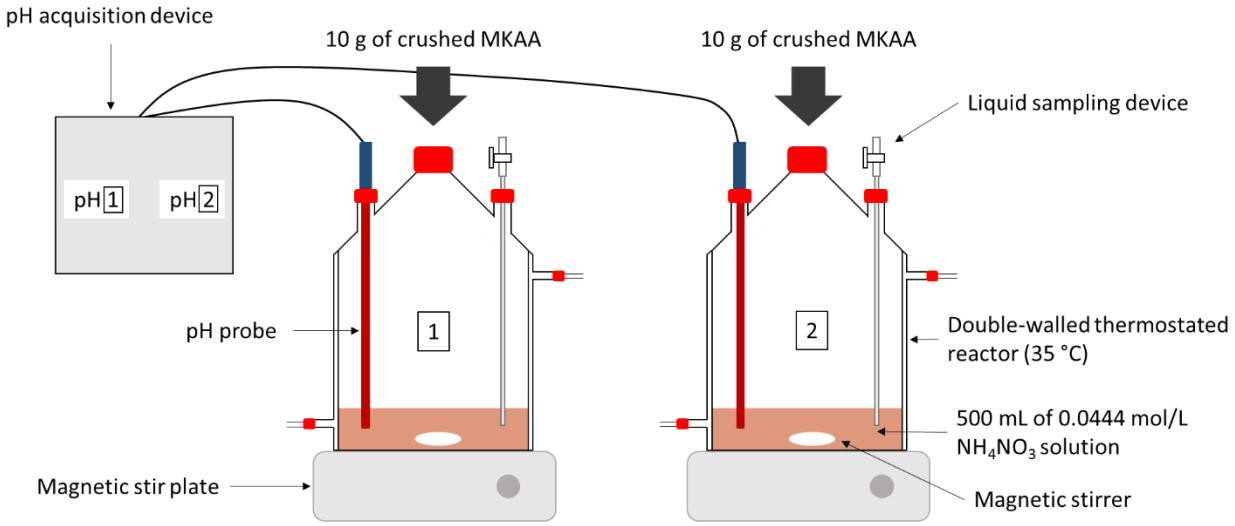

Annexe A: Experimental setup for evaluating the interaction between the MKAA and the NH_4^+ cation

References

AFNOR, 2016. NF EN 196-1. Methods of testing cement - Part 1: Determination of strength. Paris, France.

AFNOR, 2014. NF EN 206/CN. Concrete - Specification, performance, production and conformity - National addition to the standard NF EN 206. Paris, France.

AFNOR, 2012a. NF P 18-513 Addition for concrete - Metakaolin - Specifications and conformity criteria. Paris, France.

AFNOR, 2012b. NF EN 197-1. Cement - Part 1 : composition, specifications and conformity criteria for common cements. Paris, France.

Ahmed, A., Chaker, Y., Belarbi, E.H., Abbas, O., Chotard, J.N., Abassi, H.B., Van Nhien, A.N., El Hadri, M., Bresson, S., 2018. XRD and ATR/FTIR investigations of various montmorillonite clays modified by monocationic and dicationic imidazolium ionic liquids. J. Mol. Struct. 1173, 653–664. https://doi.org/10.1016/j.molstruc.2018.07.039

Aredes, F.G.M., Campos, T.M.B., Machado, J.P.B., Sakane, K.K., Thim, G.P., Brunelli, D.D., 2015. Effect of cure temperature on the formation of metakaolinite-based geopolymer. Ceram. Int. 41, 7302–7311. https://doi.org/10.1016/j.ceramint.2015.02.022

Batstone, D.J., Keller, J., Angelidaki, I., Kalyuzhnyi, S.V., Pavlostathis, S.G., Rozzi, A., Sanders, W.T.M., Siegrist, H., Vavilin, V.A., 2002. The IWA Anaerobic Digestion Model No 1 (ADM1). Water Sci. Technol. 45, 65–73.

Bertron, A., Duchesne, J., Escadeillas, G., 2005a. Accelerated tests of hardened cement pastes alteration by organic acids: analysis of the pH effect. Cem. Concr. Res. 35, 155–166. https://doi.org/10.1016/j.cemconres.2004.09.009

Bertron, A., Duchesne, J., Escadeillas, G., 2005b. Attack of cement pastes exposed to organic acids in manure. Cem. Concr. Compos. 27, 898–909. https://doi.org/10.1016/j.cemconcomp.2005.06.003

Bertron, A., Escadeillas, G., de Parseval, P., Duchesne, J., 2009. Processing of electron microprobe data from the analysis of altered cementitious materials. Cem. Concr. Res. 39, 929–935. https://doi.org/10.1016/j.cemconres.2009.06.011

Bertron, A., Peyre Lavigne, M., Patapy, C., Erable, B., 2017. Biodeterioration of concrete in agricultural, agro-food and biogas plants: state of the art and challenges. RILEM Tech. Lett. 2, 83–89. https://doi.org/10.21809/rilemtechlett.2017.42

839 Bhuiyan, M.I.H., Mavinic, D.S., Beckie, R.D., 2007. A Solubility and Thermodynamic Study of Struvite.
840 Environ. Technol. 28, 1015–1026. https://doi.org/10.1080/09593332808618857
841 Braun, R., 2007. Anaerobic digestion: a multi-faceted process for energy, environmental
842 management and rural development, in: Improvement of Crop Plants for Industrial End Uses.
843 Springer, Dordrecht, pp. 335–416. https://doi.org/10.1007/978-1-4020-5486-0_13
844 Cerrillo, M., Palatsi, J., Comas, J., Vicens, J., Bonmatí, A., 2015. Struvite precipitation as a technology
845 to be integrated in a manure anaerobic digestion treatment plant – removal efficiency,
846 crystal characterization and agricultural assessment. J. Chem. Technol. Biotechnol. 90, 1135–
847 1143. https://doi.org/10.1002/jctb.4459
848 Chae, K.-J., Choi, M.-J., Kim, K.-Y., Ajayi, F.F., Chang, I.-S., Kim, I.S., 2010. Selective inhibition of
849 methanogens for the improvement of biohydrogen production in microbial electrolysis cells.
850 Int. J. Hydrog. Energy, 3rd Asian Bio Hydrogen Symposium 35, 13379–13386.
851 https://doi.org/10.1016/j.ijhydene.2009.11.114
852 Chandra, R., Takeuchi, H., Hasegawa, T., 2012. Methane production from lignocellulosic agricultural
853 crop wastes: A review in context to second generation of biofuel production. Renew. Sustain.
854 Energy Rev. 16, 1462–1476. https://doi.org/10.1016/j.rser.2011.11.035
855 Chen, J., Yun, S., Shi, J., Wang, Z., Abbas, Y., Wang, K., Han, F., Jia, B., Xu, H., Xing, T., Li, B., 2020. Role
856 of biomass-derived carbon-based composite accelerants in enhanced anaerobic digestion:
857 Focusing on biogas yield, fertilizer utilization, and density functional theory calculations.
858 Bioresour. Technol. 307, 123204. https://doi.org/10.1016/j.biortech.2020.123204
859 Cibis, K.G., Gneipel, A., König, H., 2016. Isolation of acetic, propionic and butyric acid-forming
860 bacteria from biogas plants. J. Biotechnol. 220, 51–63.
861 https://doi.org/10.1016/j.jbiotec.2016.01.008
862 CIMbéton, 2009. Guide de prescription des ciments pour des constructions durables. Cas des bétons
863 coulés en place, Collection Technique CIMbéton.
864 Drugă, B., Ukrainczyk, N., Weise, K., Koenders, E., Lackner, S., 2018. Interaction between wastewater
865 microorganisms and geopolymer or cementitious materials: Biofilm characterization and
866 deterioration characteristics of mortars. Int. Biodeterior. Biodegrad. 134, 58–67.
867 https://doi.org/10.1016/j.ibiod.2018.08.005
868 Duan, P., Yan, C., Zhou, W., Luo, W., Shen, C., 2015. An investigation of the microstructure and
869 durability of a fluidized bed fly ash–metakaolin geopolymer after heat and acid exposure.
870 Mater. Des. 74, 125–137. https://doi.org/10.1016/j.matdes.2015.03.009
871 Elakneswaran, Y., Owaki, E., Miyahara, S., Ogino, M., Maruya, T., Nawa, T., 2016. Hydration study of
872 slag-blended cement based on thermodynamic considerations. Constr. Build. Mater. 124,
873 615–625. https://doi.org/10.1016/j.conbuildmat.2016.07.138
874 Escudero, A., Blanco, F., Lacalle, A., Pinto, M., 2015. Struvite precipitation for ammonium removal
875 from anaerobically treated effluents. J. Environ. Chem. Eng. 3, 413–419.
876 https://doi.org/10.1016/j.jece.2015.01.004
877 Evans, G.M., Furlong, J.C., 2003. Environmental Biotechnology - Theory and Application. John Wiley &
878 Sons.
879 Faucon, P., Adenot, F., Jacquinot, J.F., Petit, J.C., Cabrillac, R., Jorda, M., 1998. Long-term behaviour
880 of cement pastes used for nuclear waste disposal: review of physico-chemical mechanisms of
881 water degradation. Cem. Concr. Res. 28, 847–857. https://doi.org/10.1016/S0008-
882 8846(98)00053-2
883 Fehrenbach, H., Giegrich, J., Reinhardt, G., Sayer, U., Gretz, M., Lanje, K., Schmitz, J., 2008. Kriterien
884 einer nachhaltigen Bioenergienutzung im globalen Ma\s sstab. UBA-Forschungsbericht 206,
885 41–112.
886 Fisgativa, H., Tremier, A., Dabert, P., 2016. Characterizing the variability of food waste quality: A need
887 for efficient valorisation through anaerobic digestion. Waste Manag. 50, 264–274.
888 https://doi.org/10.1016/j.wasman.2016.01.041

889 Flemming, H.-C., Wingender, J., Szewzyk, U., Steinberg, P., Rice, S.A., Kjelleberg, S., 2016. Biofilms: an
890 emergent form of bacterial life. Nat. Rev. Microbiol. 14, 563–575.
891 https://doi.org/10.1038/nrmicro.2016.94
892 Frigon, J.-C., Guiot, S.R., 2010. Biomethane production from starch and lignocellulosic crops: a
893 comparative review. Biofuels Bioprod. Biorefining 4, 447–458.
894 https://doi.org/10.1002/bbb.229
895 Gautier, M., Muller, F., Le Forestier, L., Beny, J.-M., Guegan, R., 2010. NH4-smectite: Characterization,
896 hydration properties and hydro mechanical behaviour. Appl. Clay Sci. 49, 247–254.
897 https://doi.org/10.1016/j.clay.2010.05.013
898 Girou, A., Roques, H., 1971. Etude des cinétiques de précipitation des carbonates de calcium. Bull.
899 Assoc. Géographes Fr. 48, 227–233. https://doi.org/10.3406/bagf.1971.7651
900 Grengg, C., Ukrainczyk, N., Koraimann, G., Mueller, B., Dietzel, M., Mittermayr, F., 2020. Long-term in
901 situ performance of geopolymer, calcium aluminate and Portland cement-based materials
902 exposed to microbially induced acid corrosion. Cem. Concr. Res. 131, 106034.
903 https://doi.org/10.1016/j.cemconres.2020.106034
904 Gruyaert, E., Van den Heede, P., Maes, M., De Belie, N., 2012. Investigation of the influence of blast-
905 furnace slag on the resistance of concrete against organic acid or sulphate attack by means
906 of accelerated degradation tests. Cem. Concr. Res. 42, 173–185.
907 https://doi.org/10.1016/j.cemconres.2011.09.009
908 Hagos, K., Zong, J., Li, D., Liu, C., Lu, X., 2017. Anaerobic co-digestion process for biogas production:
909 Progress, challenges and perspectives. Renew. Sustain. Energy Rev. 76, 1485–1496.
910 https://doi.org/10.1016/j.rser.2016.11.184
911 Han, F., Yun, S., Zhang, C., Xu, H., Wang, Z., 2019. Steel slag as accelerant in anaerobic digestion for
912 nonhazardous treatment and digestate fertilizer utilization. Bioresour. Technol. 282, 331–
913 338. https://doi.org/10.1016/j.biortech.2019.03.029
914 Han, G., Shin, S.G., Lee, J., Lee, C., Jo, M., Hwang, S., 2016. Mesophilic Acidogenesis of Food Waste-
915 Recycling Wastewater: Effects of Hydraulic Retention Time, pH, and Temperature. Appl.
916 Biochem. Biotechnol. 180, 980–999. https://doi.org/10.1007/s12010-016-2147-z
917 Holliger, C., Alves, M., Andrade, D., Angelidaki, I., Astals, S., Baier, U., Bougrier, C., Buffière, P.,
918 Carballa, M., de Wilde, V., Ebertseder, F., Fernández, B., Ficara, E., Fotidis, I., Frigon, J.-C., de
919 Laclos, H.F., Ghasimi, D.S.M., Hack, G., Hartel, M., Heerenklage, J., Horvath, I.S., Jenicek, P.,
920 Koch, K., Krautwald, J., Lizasoain, J., Liu, J., Mosberger, L., Nistor, M., Oechsner, H., Oliveira,
921 J.V., Paterson, M., Pauss, A., Pommier, S., Porqueddu, I., Raposo, F., Ribeiro, T., Rüsch Pfund,
922 F., Strömberg, S., Torrijos, M., van Eekert, M., van Lier, J., Wedwitschka, H., Wierinck, I.,
923 2016. Towards a standardization of biomethane potential tests. Water Sci. Technol. 74,
924 2515–2522. https://doi.org/10.2166/wst.2016.336
925 Holm-Nielsen, J.B., Al Seadi, T., Oleskowicz-Popiel, P., 2009. The future of anaerobic digestion and
926 biogas utilization. Bioresour. Technol., OECD Workshop: Livestock Waste Treatment Systems
927 of the Future: A Challenge to Environmental Quality, Food Safety, and Sustainability 100,
928 5478–5484. https://doi.org/10.1016/j.biortech.2008.12.046
929 Huang, X., Yun, S., Zhu, J., Du, T., Zhang, C., Li, X., 2016. Mesophilic anaerobic co-digestion of aloe
930 peel waste with dairy manure in the batch digester: Focusing on mixing ratios and digestate
931 stability. Bioresour. Technol. 218, 62–68. https://doi.org/10.1016/j.biortech.2016.06.070
932 Hunger, M., 1996. Multinuclear solid-state NMR studies of acidic and non-acidic hydroxyl protons in
933 zeolites. Solid State Nucl. Magn. Reson. 6, 1–29. https://doi.org/10.1016/0926-
934 2040(95)01201-X
935 Jacobs, W.P.J.H., de Haan, J.W., van de Ven, L.J.M., van Santen, R.A., 1993. Interaction of ammonia
936 with Broensted acid sites in different cages of zeolite Y as studied by proton MAS NMR. J.
937 Phys. Chem. 97, 10394–10402. https://doi.org/10.1021/j100142a022
938 Juenger, M.C.G., Snellings, R., Bernal, S.A., 2019. Supplementary cementitious materials: New
939 sources, characterization, and performance insights. Cem. Concr. Res. 122, 257–273.
940 https://doi.org/10.1016/j.cemconres.2019.05.008

941 Khan, H.A., Castel, A., Khan, M.S.H., 2020. Corrosion investigation of fly ash based geopolymer
942 mortar in natural sewer environment and sulphuric acid solution. Corros. Sci. 108586.
943 https://doi.org/10.1016/j.corsci.2020.108586
944 Khan, H.A., Castel, A., Khan, M.S.H., 2017. Performance Evaluation of Geopolymer against In Situ
945 Aggressive Sewer Environment, in: Concrete 2017. Presented at the Concrete 2017, Adelaïde,
946 Australia.
947 Khan, H.A., Khan, M.S.H., Castel, A., Sunarho, J., 2018. Deterioration of alkali-activated mortars
948 exposed to natural aggressive sewer environment. Constr. Build. Mater. 186, 577–597.
949 https://doi.org/10.1016/j.conbuildmat.2018.07.137
950 Kim, J., Park, C., Kim, T.-H., Lee, M., Kim, S., Kim, S.-W., Lee, J., 2003. Effects of various pretreatments
951 for enhanced anaerobic digestion with waste activated sludge. J. Biosci. Bioeng. 95, 271–275.
952 https://doi.org/10.1016/S1389-1723(03)80028-2
953 Kim, M., Gomec, C.Y., Ahn, Y., Speece, R.E., 2003. Hydrolysis and acidogenesis of particulate organic
954 material in mesophilic and thermophilic anaerobic digestion. Environ. Technol. 24, 1183–
955 1190. https://doi.org/10.1080/09593330309385659
956 Koenig, A., Dehn, F., 2016. Biogenic acid attack on concretes in biogas plants. Biosyst. Eng. 147, 226–
957 237. https://doi.org/10.1016/j.biosystemseng.2016.03.007
958 Koenig, A., Dehn, F., 2015. Acid Resistance of Ultra High-Performance Concrete (UHPC), in: Sobolev,
959 K., Shah, S.P. (Eds.), Nanotechnology in Construction. Springer International Publishing,
960 Cham, pp. 317–323. https://doi.org/10.1007/978-3-319-17088-6_41
961 Kothari, R., Pandey, A.K., Kumar, S., Tyagi, V.V., Tyagi, S.K., 2014. Different aspects of dry anaerobic
962 digestion for bio-energy: An overview. Renew. Sustain. Energy Rev. 39, 174–195.
963 https://doi.org/10.1016/j.rser.2014.07.011
964 Kuypers, M.M.M., Marchant, H.K., Kartal, B., 2018. The microbial nitrogen-cycling network. Nat. Rev.
965 Microbiol. 16, 263–276. https://doi.org/10.1038/nrmicro.2018.9
966 Lastella, G., Testa, C., Cornacchia, G., Notornicola, M., Voltasio, F., Sharma, V.K., 2002. Anaerobic
967 digestion of semi-solid organic waste: biogas production and its purification. Energy Convers.
968 Manag. 43, 63–75. https://doi.org/10.1016/S0196-8904(01)00011-5
969 Lesteur, M., Bellon-Maurel, V., Gonzalez, C., Latrille, E., Roger, J.M., Junqua, G., Steyer, J.P., 2010.
970 Alternative methods for determining anaerobic biodegradability: A review. Process Biochem.
971 45, 431–440. https://doi.org/10.1016/j.procbio.2009.11.018
972 Li, K., Liu, R., Sun, C., 2015. Comparison of anaerobic digestion characteristics and kinetics of four
973 livestock manures with different substrate concentrations. Bioresour. Technol. 198, 133–140.
974 https://doi.org/10.1016/j.biortech.2015.08.151
975 Limoli, A., Langone, M., Andreottola, G., 2016. Ammonia removal from raw manure digestate by
976 means of a turbulent mixing stripping process. J. Environ. Manage. 176, 1–10.
977 https://doi.org/10.1016/j.jenvman.2016.03.007
978 Lin, L., Lei, Z., Wang, L., Liu, X., Zhang, Y., Wan, C., Lee, D.-J., Tay, J.H., 2013. Adsorption mechanisms
979 of high-levels of ammonium onto natural and NaCl-modified zeolites. Sep. Purif. Technol.
980 103, 15–20. https://doi.org/10.1016/j.seppur.2012.10.005
981 Liu, C., Yuan, X., Zeng, G., Li, W., Li, J., 2008. Prediction of methane yield at optimum pH for anaerobic
982 digestion of organic fraction of municipal solid waste. Bioresour. Technol. 99, 882–888.
983 https://doi.org/10.1016/j.biortech.2007.01.013
984 Lothenbach, B., Scrivener, K., Hooton, R.D., 2011. Supplementary cementitious materials. Cem.
985 Concr. Res., Conferences Special: Cement Hydration Kinetics and Modeling, Quebec City,
986 2009 & CONMOD10, Lausanne, 2010 41, 1244–1256.
987 https://doi.org/10.1016/j.cemconres.2010.12.001
988 Luukkonen, T., Sarkkinen, M., Kemppainen, K., Rämö, J., Lassi, U., 2016. Metakaolin geopolymer
989 characterization and application for ammonium removal from model solutions and landfill
990 leachate. Appl. Clay Sci. 119, 266–276. https://doi.org/10.1016/j.clay.2015.10.027

Magniont, C., Coutand, M., Bertron, A., Cameleyre, X., Lafforgue, C., Beaufort, S., Escadeillas, G., 2011. A new test method to assess the bacterial deterioration of cementitious materials. Cem. Concr. Res. 41, 429–438. https://doi.org/10.1016/j.cemconres.2011.01.014

Marañón, E., Ulmanu, M., Fernández, Y., Anger, I., Castrillón, L., 2006. Removal of ammonium from aqueous solutions with volcanic tuff. J. Hazard. Mater. 137, 1402–1409. https://doi.org/10.1016/j.jhazmat.2006.03.069

McCarty, P.L., 1964. Anaerobic Waste treatment Fundamentals. Public Works 95, 66.

Mookherjee, M., Welch, M.D., Pollès, L.L., Redfern, S.A.T., Harlov, D.E., 2005. Ammonium ion behaviour in feldspar: variable-temperature infrared and 2H NMR studies of synthetic buddingtonite, N(D,H)4AlSi3O8. Phys. Chem. Miner. 32, 126–131. https://doi.org/10.1007/s00269-005-0455-x

Morandeau, A., Thiéry, M., Dangla, P., 2014. Investigation of the carbonation mechanism of CH and C-S-H in terms of kinetics, microstructure changes and moisture properties. Cem. Concr. Res. 56, 153–170. https://doi.org/10.1016/j.cemconres.2013.11.015

Nathalie Bachmann, E.S.A., 2013. 8 - Design and engineering of biogas plants, in: Wellinger, A., Murphy, J., Baxter, D. (Eds.), The Biogas Handbook, Woodhead Publishing Series in Energy. Woodhead Publishing, pp. 191–211. https://doi.org/10.1533/9780857097415.2.191

O'Connor, S.J., MacKenzie, K.J.D., Smith, M.E., Hanna, J.V., 2010. Ion exchange in the charge-balancing sites of aluminosilicate inorganic polymers. J. Mater. Chem. 20, 10234–10240. https://doi.org/10.1039/C0JM01254H

Oral, Ç.M., Ercan, B., 2018. Influence of pH on morphology, size and polymorph of room temperature synthesized calcium carbonate particles. Powder Technol. 339, 781–788. https://doi.org/10.1016/j.powtec.2018.08.066

Oueslati, O., Duchesne, J., 2012. The effect of SCMs and curing time on resistance of mortars subjected to organic acids. Cem. Concr. Res. 42, 205–214. https://doi.org/10.1016/j.cemconres.2011.09.017

Perlot, C., Verdier, J., Carcassès, M., 2006. Influence of cement type on transport properties and chemical degradation: application to nuclear waste storage. Mater. Struct. 39, 511–523.

Pouhet, R., 2015. Formulation and durability of metakaolin-based geopolymers (phd). Université de Toulouse, Université Toulouse III - Paul Sabatier.

Pouhet, R., Cyr, M., Bucher, R., 2019. Influence of the initial water content in flash calcined metakaolin-based geopolymer. Constr. Build. Mater. 201, 421–429. https://doi.org/10.1016/j.conbuildmat.2018.12.201

Rasi, S., 2009. Biogas composition and upgrading to biomethane (Jyväskylä studies in Biological and Environmental Science). University of Jyväskylä, Finland.

Roosz, C., Vieillard, P., Blanc, P., Gaboreau, S., Gailhanou, H., Braithwaite, D., Montouillout, V., Denoyel, R., Henocq, P., Madé, B., 2018. Thermodynamic properties of C-S-H, C-A-S-H and M-S-H phases: Results from direct measurements and predictive modelling. Appl. Geochem. 92, 140–156. https://doi.org/10.1016/j.apgeochem.2018.03.004

San Nicolas, R., Cyr, M., Escadeillas, G., 2013. Characteristics and applications of flash metakaolins. Appl. Clay Sci. 83–84, 253–262. https://doi.org/10.1016/j.clay.2013.08.036

Scrivener, K., Snellings, R., Lothenbach, B., 2016. A Practical Guide to Microstructural Analysis of Cementitious Materials. CRC Press.

Ševčík, R., Pérez-Estébanez, M., Viani, A., Šašek, P., Mácová, P., 2015. Characterization of vaterite synthesized at various temperatures and stirring velocities without use of additives. Powder Technol. 284, 265–271. https://doi.org/10.1016/j.powtec.2015.06.064

Singh, B., Ishwarya, G., Gupta, M., Bhattacharyya, S.K., 2015. Geopolymer concrete: A review of some recent developments. Constr. Build. Mater. 85, 78–90. https://doi.org/10.1016/j.conbuildmat.2015.03.036

Snellings, R., Chwast, J., Cizer, Ö., De Belie, N., Dhandapani, Y., Durdzinski, P., Elsen, J., Haufe, J., Hooton, D., Patapy, C., Santhanam, M., Scrivener, K., Snoeck, D., Steger, L., Tongbo, S., Vollpracht, A., Winnefeld, F., Lothenbach, B., 2018. RILEM TC-238 SCM recommendation on

hydration stoppage by solvent exchange for the study of hydrate assemblages. Mater. Struct. 51, 172. https://doi.org/10.1617/s11527-018-1298-5
Stepkowska, E.T., Pérez-Rodríguez, J.L., Sayagués, M.J., Martínez-Blanes, J.M., 2003. Calcite, vaterite and aragonite forming on cement hydration from liquid and gaseous phase. J. Therm. Anal. Calorim. 73, 247–269. https://doi.org/10.1023/A:1025158213560
Tai, C.Y., Chen, F.-B., 1998. Polymorphism of CaCO3, precipitated in a constant-composition environment. AIChE J. 44, 1790–1798. https://doi.org/10.1002/aic.690440810
The European Parliament, The European Union Council, 2009. Directive 2009/28/EC, 140.
The European Parliament, The European Union Council, 2001. Directive 2001/77/EC.
Voegel, C., 2017. Impact biochimique des effluents agricoles et agroindustriels sur les structures/ouvrages en béton dans la filière de valorisation par méthanisation (ou digestion anaérobie). Institut National Polytechnique de Toulouse (INP Toulouse), Toulouse, France. http://www.theses.fr/2017INPT0044.
Voegel, C., Bertron, A., Erable, B., 2016. Mechanisms of cementitious material deterioration in biogas digester. Sci. Total Environ. 571, 892–901. https://doi.org/10.1016/j.scitotenv.2016.07.072
Voegel, C., Bertron, A., Erable, B., 2015. Biodeterioration of cementitious materials in biogas digester. Matér. Tech. 103, 202. https://doi.org/10.1051/mattech/2015023
Voegel, C., Durban, N., Bertron, A., Landon, Y., Erable, B., 2019a. Evaluation of microbial proliferation on cementitious materials exposed to biogas systems. Environ. Technol. 1–11. https://doi.org/10.1080/09593330.2019.1567610
Voegel, C., Giroudon, M., Bertron, A., Patapy, C., Peyre Lavigne, M., Verdier, T., Erable, B., 2019b. Cementitious materials in biogas systems: Biodeterioration mechanisms and kinetics in CEM I and CAC based materials. Cem. Concr. Res. 124, 105815. https://doi.org/10.1016/j.cemconres.2019.105815
Wang, H., Li, H., Yan, F., 2005. Synthesis and mechanical properties of metakaolinite-based geopolymer. Colloids Surf. Physicochem. Eng. Asp. 268, 1–6. https://doi.org/10.1016/j.colsurfa.2005.01.016
Wang, P., Wang, H., Qiu, Y., Ren, L., Jiang, B., 2018. Microbial characteristics in anaerobic digestion process of food waste for methane production–A review. Bioresour. Technol., Bioconversion of Food Wastes 248, 29–36. https://doi.org/10.1016/j.biortech.2017.06.152
Wang, Q., Yang, Y., Yu, C., Huang, H., Kim, M., Feng, C., Zhang, Z., 2011. Study on a fixed zeolite bioreactor for anaerobic digestion of ammonium-rich swine wastes. Bioresour. Technol. 102, 7064–7068. https://doi.org/10.1016/j.biortech.2011.04.085
Wang, Z., Yun, S., Xu, H., Wang, C., Zhang, Y., Chen, J., Jia, B., 2019. Mesophilic anaerobic co-digestion of acorn slag waste with dairy manure in a batch digester: Focusing on mixing ratios and bio-based carbon accelerants. Bioresour. Technol. 286, 121394. https://doi.org/10.1016/j.biortech.2019.121394
Weiland, P., 2010. Biogas production: current state and perspectives. Appl. Microbiol. Biotechnol. 85, 849–860. https://doi.org/10.1007/s00253-009-2246-7
Wianglor, K., Sinthupinyo, S., Piyaworapaiboon, M., Chaipanich, A., 2017. Effect of alkali-activated metakaolin cement on compressive strength of mortars. Appl. Clay Sci. 141, 272–279. https://doi.org/10.1016/j.clay.2017.01.025
Wray, J.L., Daniels, F., 1956. Precipitation of Calcite and Aragonite. J. Am. Chem. Soc. 79, 2031–2034.
Xu, H., Li, Y., Hua, D., Mu, H., Zhao, Y., Chen, G., 2019. Methane production from the anaerobic digestion of substrates from corn stover: Differences between the stem bark, stem pith, and leaves. Sci. Total Environ. 694, 133641. https://doi.org/10.1016/j.scitotenv.2019.133641
Xu, H., Yun, S., Wang, C., Wang, Z., Han, F., Jia, B., Chen, J., Li, B., 2020. Improving performance and phosphorus content of anaerobic co-digestion of dairy manure with aloe peel waste using vermiculite. Bioresour. Technol. 301, 122753. https://doi.org/10.1016/j.biortech.2020.122753
Yariv, S., 1985. Study of the adsorption of organic molecules on clay minerals by differential thermal analysis. Thermochim. Acta 88, 49–68. https://doi.org/10.1016/0040-6031(85)85414-9

Yenigün, O., Demirel, B., 2013. Ammonia inhibition in anaerobic digestion: A review. Process Biochem. 48, 901–911. https://doi.org/10.1016/j.procbio.2013.04.012

Yu, H.-Q., Fang, H.H.P., 2002. Acidogenesis of dairy wastewater at various pH levels. Water Sci. Technol. 45, 201–206.

Yun, S., Fang, W., Du, T., Hu, X., Huang, X., Li, X., Zhang, C., Lund, P.D., 2018. Use of bio-based carbon materials for improving biogas yield and digestate stability. Energy 164, 898–909. https://doi.org/10.1016/j.energy.2018.09.067

Yun, S., Zhang, C., Wang, Y., Zhu, J., Huang, X., Du, T., Li, X., Wei, Y., 2019. Synergistic effects of Fe salts and composite additives on anaerobic digestion of dairy manure. Int. Biodeterior. Biodegrad. 136, 82–90. https://doi.org/10.1016/j.ibiod.2018.10.011

Zhang, C., Yun, S., Li, X., Wang, Z., Xu, H., Du, T., 2018. Low-cost composited accelerants for anaerobic digestion of dairy manure: Focusing on methane yield, digestate utilization and energy evaluation. Bioresour. Technol. 263, 517–524. https://doi.org/10.1016/j.biortech.2018.05.042